REPUBLIC OF TURKEY
ADANA ALPARSLAN TÜRKEŞ SCIENCE AND TECHNOLOGY UNIVERSITY

GRADUATE SCHOOL OF NATURAL AND APPLIED SCIENCES
DEPARTMENT OF NANOTECHNOLOGY AND ENGINEERING SCIENCES

STUDY OF MORPHOLOGY AND DYE EFFECTS ON THE EFFICIENCY OF CdS–BASED HYBRID SOLAR CELLS

AHMET ÜNVERDİ
MASTER OF SCIENCE

ADANA 2020

REPUBLIC OF TURKEY
ADANA ALPARSLAN TÜRKEŞ SCIENCE AND TECHNOLOGY UNIVERSITY

GRADUATE SCHOOL OF NATURAL AND APPLIED SCIENCES
DEPARTMENT OF NANOTECHNOLOGY AND ENGINEERING SCIENCES

STUDY OF MORPHOLOGY AND DYE EFFECTS ON THE EFFICIENCY OF CdS–BASED HYBRID SOLAR CELLS

AHMET ÜNVERDİ
MASTER OF SCIENCE

SUPERVISOR
ASSOC. PROF. DR. SALİH YILMAZ

ADANA 2020

I hereby declare that all information in this thesis has been obtained and presented in accordance with academic rules and ethical conduct. I also declare that, as required by these rules and conduct, I have fully cited and referenced all information that is not original to this work.

Ahmet ÜNVERDİ

ABSTRACT

STUDY OF MORPHOLOGY AND DYE EFFECTS ON THE EFFICIENCY OF CdS–BASED HYBRID SOLAR CELLS

Ahmet ÜNVERDİ

Department of Nanotechnology and Engineering Sciences

Supervisor: Assoc. Prof. Dr. Salih YILMAZ

July 2020, 54 pages

In this project study, some properties of hybrid solar cells (HSCs) formed by CdS samples that were grown by the different methods (spray pyrolysis, chemical bath deposition, doctor blade and hydrothermal methods) and in different morphologies (thin film, powder and nanosphere) were investigated. Additionally, structural, morphological, optical and electrical properties of HSCs based on CdS samples whose surfaces were modified by diverse dyes (Eosin–Y, D205, N719 and N3) were studied. X–ray Diffraction (XRD) results showed the crystallization of CdS samples in the polycrystalline structure. Scanning Electron Microscopy (SEM) conclusions indicated the homogeneous coverage of P3HT on the produced CdS samples with different morphologies. Energy dispersive X–ray Spectroscopy (EDS) approved the presence of Cd and S atoms in CdS structure. It was concluded that the transmittance data of synthesized CdS specimens were quite good and hence, they can be used for the solar cell (SC) applications. It was observed that the band gaps of the prepared CdS samples were based on the method used. It was seen that the peak intensities of the absorbance of CdS-based heterostructures generally increased with the modification of CdS surface by dyes. It was observed from room temperature photoluminescence (RTPL) outputs that CdS samples produced by different routes exhibited various defects. Furthermore, it was determined that the peak intensities in the photoluminescence (PL) spectra of CdS–based heterostructures generally decreased after dye modification of CdS surface. From the electrical measurements, it was seen that CdS–based heterostructures displayed an obvious photovoltaic effect. It was observed that both CdS samples grown in the different morphology and the surface modified by diverse dyes had different power conversion efficiency (PCE) values. The highest efficiency value was appeared for CdS samples with the nanosphere morphology and modified by N719 dye as 0.881%. Thus, it can be deduced that in addition to different morphology, modification by diverse dyes also leads to an important variation on the SC efficiency.

Keywords: CdS, morphology effect, P3HT, dye effect, hybrid solar cell

ÖZET

MORFOLOJİ VE BOYA ETKİSİNİN CdS–TABANLI HİBRİT GÜNEŞ PİLLERİNİN VERİMLİLİĞİ ÜZERİNE OLAN ETKİLERİNİN ARAŞTIRILMASI

Ahmet ÜNVERDİ

Nanoteknoloji ve Mühendislik Bilimleri Anabilim Dalı

Danışman: Doç. Dr. Salih YILMAZ

Temmuz 2020, 54 sayfa

Bu proje çalışmasında, farklı yöntemlerle (kimyasal püskürtme, kimyasal banyoda çökeltme, doktor bıçağı ve hidrotermal yöntem) farklı morfolojili (ince film, toz ve nanoküre) olacak şekilde büyütülen CdS örneklerle oluşturulan hibrit güneş hücrelerinin bazı özellikleri incelendi. Ayrıca farklı boyalarla (Eosin–Y, D205, N719 ve N3) yüzeyi modifiye edilmiş CdS örneklerle üretilen hibrit güneş pillerinin yapısal, morfolojik, optik ve elektriksel özellikleri araştırıldı. X–ışınları kırınım (XRD) sonuçları CdS örneklerinin polikristal yapıda kristalleştiğini gösterdi. Taramalı elektron mikroskobu (SEM) sonuçları, üretilen farklı morfolojili CdS örnekler üzerine homojen bir P3HT katmanının kaplandığını gösterdi. Enerji dağılımlı X–ışını spektroskopisi (EDS) CdS yapısı içerisinde Cd ve S atomlarının var olduğunu ispatladı. Üretilen CdS örneklerin geçirgenlik sonuçlarının genel olarak iyi olduğu ve dolayısıyla güneş pili uygulamaları için kullanılabileceği sonucuna varıldı. Büyütülen CdS örneklerin bant aralık değerlerinin ise, üretilen yönteme göre farklılık gösterdiği belirlendi. CdS yüzeyinin boya modifikasyonuyla beraber, soğurma pik şiddetlerinde genellikle artışlar olduğu görüldü. Oda sıcaklık fotolüminesans (RTPL) sonuçlarından, farklı yöntemlerle üretilen CdS örneklerin farklı dalga boylarında farklı kusurlar sergilediği gözlendi. Ayrıca CdS tabanlı heteroyapıların fotolüminesans pik şiddetlerinde boya modifikasyonuyla beraber çoğunlukla azalma olduğu tespit edildi. Elektriksel ölçümlerden, CdS tabanlı heteroyapıların açık bir şekilde fotovoltaik etki sergiledikleri görüldü. Hem farklı morfolojide büyütülen hem de farklı boyalarla yüzeyi modifiye edilen CdS örneklerin farklı güneş pili verimlerine sahip oldukları gözlendi. En yüksek güneş hücre verim değeri, nanoküre morfolojisine sahip ve N719 yüzey boya modifikasyonu yapılmış CdS örnekler için % 0,881 ile ortaya çıktı. Böylece farklı morfolojinin yanı sıra farklı boyayla CdS yüzeyinin modifikasyonunun güneş hücre verimlerinde önemli değişikliklere yol açtığı sonucuna varıldı.

Anahtar Kelimeler: CdS, morfoloji etkisi, P3HT, boya etkisi, hibrit güneş pili

First and foremost, I am dedicating this thesis to our Almighty God, Allah (Great is His Majesty), the source of my wisdom, strong pillar, inspiration and knowledge.

To our Prophet Muhammad (peace and blessings be upon him), and all the other Prophets, four Great Caliphs, all Saints and Scholars for spreading Islam and doing their best for humanity.

To our Ancestors; Turkish Rulers & Ottoman Sultans and past, current & future Presidents of the Republic of Turkey due to their struggle for both independence and protection.

To my dad, mom, and grandfather and to the memory of my grandparents, for always being there.

To my family, nieces & nephews and my future wife & children.

To my relatives, teachers, friends and those who touched my life since my conception.

To those who do the best for the good of all humankind and to scientists, doctors, teachers, nurses, soldiers etc.

*And lastly, to my beloved hamsters **Zibidi** & **Pamuk**, their granddaughter **Pakize** and to my cat **Karagöz** that passed away.*

-thehamsterfather-

ACKNOWLEDGEMENTS

I would like to express my endless thanks to my supervisor, Assoc. Prof. Dr. Salih YILMAZ, who did not withhold his help not only for my educational life, also for my personal life and who is the biggest encourager in my thesis writing while doing the best in transferring his knowledge and experience. I am honored to have the opportunity for being his student and I am very proud of it.

I am very grateful to Prof. Dr. Emin BACAKSIZ, Prof. Dr. Murat TOMAKİN and Assoc. Prof. Dr. İsmail POLAT for their supports on the synthesis of CdS thin films by spray pyrolysis and device characterizations.

I would like to extend my sincere thanks to my former class/housemates Mr. Şahin ÇAĞRET and Mr. Said YALÇIN, to my friend Mrs. Hirah Fatimah, and to my beloved yokemate Mr. Evren TOKER for their moral supports during my both personal and educational life. Also, I would like to thank to those who has touched my life since my conception.

Once for all, special thanks to my parents due to their lifelong moral and financial supports. Having them as my parents is the most honorable thing within my life and I feel so blessed due to it. I would like to express my deepest gratitude to them for instilling me with a strong passion for learning, besides passing down the honesty and perseverance to me. They have never grumbled about my education cost regardless of their tight budget, nevertheless, they sacrificed too much for me. I feel so honored to be graduating from Adana Alparslan Türkeş Science and Technology University with Master's Degree. This achievement would not have been possible without their support.

This thesis was financially supported by TÜBİTAK (Scientific and Technological Research Council of Turkey) by a project number of 116F296.

TABLE OF CONTENTS

LIST OF FIGURES

LIST OF TABLES

NOMENCLATURE

a, c	: Lattice parameters
Ag	: Silver
Al	: Aluminum
Au	: Gold
CBD	: Chemical bath deposition
Cd	: Cadmium
$CdCl_2$	: Cadmium Chloride
$Cd(NO_3)_2.4H_2O$	: Cadmium Nitrate Tetrahydrate
CdS	: Cadmium Sulfide
$(NH_2)_2CS$	: Thiourea
$CdTe$	: Cadmium Telluride
$CIGS$	: Copper indium gallium (di) selenide ($Cu(InGa)Se_2$)
D	: Crystallite size
$D-A$	: Donor–acceptor
$DSSCs$	: Dye sensitized solar cells
EDS	: Energy dispersive X–ray spectroscopy
EQE	: External quantum efficiency
ε_r	: Dielectric constant
FF	: Fill factor
FTO	: Fluorine–doped tin oxide – coated glass substrates
$FWHM, \beta$	: Full width at half maximum
$\hbar$	: Reduced Planck constant
$HOMO$	: Highest occupied molecular orbital
$HSCs$	: Hybrid solar cells
I_{Cd}	: Cadmium interstitial
In	: Indium
I_S	: Sulphur interstitial
I_{sc}	: Short circuit current

ITO : Indium tin oxide – coated glass substrates

J_0 : Saturation current density

J_m : Maximum power point current density

J_{ph} : Photo–generated current density

J_{sc} : Short circuit current density

k_B : Boltzmann constant

λ : Wavelength

$LUMO$: Lowest unoccupied molecular orbital

η_{abs} : Absorption yield of the device

η_{cc} : Efficiency of charge collection at the electrodes

η_{diff} : Ability of an exciton to diffuse to a D–A interface

η_{diss} : Exciton dissociation yield

η_{tr} : Efficiency of charge carrier transport throughout the device

NH_4Cl : Ammonium Chloride

NH_4OH : Ammonia solution (25%)

nm : Nanometer

μm : Micrometer

$NRAs$: Nanorod arrays

OPV : Organic photovoltaic

$P3HT$: Poly(3-hexylthiophene-2,5-diyl)

$PCBM$: Phenyl-C_{61}-Butyric-Acid-Methyl-Ester

PCE, η : Power conversion efficiency

$PEDOT:PSS$: Poly(ethylene dioxythiophene):poly(styrene sulfonate)

P_{in} : Incident input power

PL : Photoluminescence

P_{max} : Maximum power

PV : Photovoltaic

q : Electric charge

R_s : Series resistance

R_{sh} : Shunt resistance

RT : Room temperature

$RTPL$: Room temperature photoluminescence

S	: Sulphur
SC	: Solar cell
SEM	: Scanning electron microscopy
Si	: Silicon
T	: Temperature
TCO	: Transparent conducting oxide
TiO_2	: Titanium dioxide
$TNAs$	: Titanium dioxide nanotube arrays
$TX-100$	: Triton
UV	: Ultraviolet
VIS	: Visible region
V_{Cd}	: Cadmium vacancy
V_m	: Maximum power voltage
V_{oc}	: Open circuit voltage
V_S	: Sulphur vacancy
XRD	: X–ray Diffraction
ZnO	: Zinc oxide
θ	: Bragg diffraction angle

1. INTRODUCTION

1.1. Brief Information of Today's Solar Cells

The increasing energy demand of today's world and the negative effects of fossil fuels on climate change have increased scientists' interest in renewable and clean energy sources. As a promising example, photovoltaic (PV) cells have been widely researched recently. According to the material types that are used, SCs have been considered under three fundamental topics: organic–organic, inorganic–inorganic and HSCs. Environmental stability, excellent load–bearing properties and up to 25% PCE of crystalline silicon–based PVs are an important part of the photovoltaic market today. However, compared to traditional production methods, crystalline silicon–based SCs could not constitute a significant part of today's world on renewable energy sources due to their high production costs (Christoph, 2004). On the other hand, the high costs of purification techniques used to obtain high purity silicon also led to a decrease in the interest of silicon–based photovoltaics. Therefore, SCs consisting of inorganic thin film layers were produced alternatively to crystalline silicon–based SCs. In these devices, there is a relationship between the battery efficiency and the thickness of the produced semiconductor layer. Although thinly obtained semiconductor material causes a reduction in costs, this phenomenon leads to a decrease in PCE due to the limited crystal quality of the semiconductor thin film. CIGS and CdTe are semiconductor compounds that are used for this technology today and significant contributions were made to the photovoltaic industry with this technology. In the fabrication of these semiconductor compounds, rare materials are needed although these devices decreases the production cost of SCs. Recently, studies on low–cost photovoltaic batteries have increased researchers' interest in organic materials. The discovery of conductive and semiconductor organic materials has paved the way for new and thrilling potential in optoelectronic device field. The most important benefit of using organic materials is the opportunity to easily fabricate PV devices via solution–based methods that are cheap and extremely efficient. However, the fact that organic semiconductors have a very large absorption coefficient requires the production of very thin organic films. The use of low–cost production techniques with this reduction in the amount of materials used makes organic semiconductors one of the most important potentials of the photovoltaic market (Wright & Uddin, 2012). In the last five years, studies on the efficiency of organic photovoltaic (OPV) batteries have been found to reach 10% efficiency. This PCE value has

been acknowledged as a milestone in organic–based photovoltaics. In addition to the use of the above–mentioned advantages, noteworthy increments in efficiency gave rise to the fabrication of some commercial OPV devices (Green, Emery, Hishikawa, Warta, & Dunlop, 2014).

1.2. Hybrid Solar Cells

Organic–inorganic HSCs are fabricated by combination of inorganic materials and organic conjugated polymer with the advantages of both material groups. The fact that the charge carriers move faster in inorganic materials and the low cost production of semiconductor polymers and the ability to absorb incoming light cause such materials to be combined. Absorption of the excitons in the inorganic material attains photogeneration of charge carriers. In OPV devices, the increasing absorption of light by an inorganic acceptor is inclined to be better than that of Phenyl-C_{61}-Butyric-Acid-Methyl-Ester (PCBM). In addition, the band gap and hence the absorption profile of the nanoparticle are altered by quantum confinement due to the alteration of shape and size of the inorganic nanoparticle. This allows the selection of spectral window of the completing absorption profile. Since the transfer rate of inorganic quantum dots to organic semiconductors has been seen in order of picoseconds and is higher than that of competing recombination mechanisms, between donor and acceptor, an efficient charge transfer can be obtained. The physical measurements of inorganic oxide semiconductors can be adjusted by fabrication techniques to obtain vertically well aligned nanostructures. Efficient excitonic dissociation and electron transporting paths can be achieved simultaneously in devices obtained by this adjustment. These assets could be gathered while maintaining solution processability that leads to low cost fabrication and high throughput. It is already known that inorganic acceptors used in HSCs have advantages, however, the efficiency of these HSCs could not reach that of polymer:fullerene OPV devices. The most important reasons for this conflict are associated with surface chemistry and nanomorphology (Wright & Uddin, 2012; Jabeen et al., 2017). The operation and fabrication of HSCs are not different from that of organic SCs at all. The only distinction between both of them is that inorganic semiconductor material is used instead of organic electron acceptor material as it is already mentioned above. This inorganic material can be quantum dots distributed inside the polymer matrix or morphologies such as nanosphere, nanowire and nanoparticle. The most of the HSCs are of planar nature and contain the photoactive layer formed between electrodes with two different work functions (anode and cathode). The anode

electrode consists of a semipermeable oxide layer and Indium tin oxide (ITO) or Fluorine–doped tin oxide coated glass substrates (FTO) are generally used for this purpose. The task of this layer is making the transition process of light and accumulating the holes in the device. A conductive polymer mixture of poly(ethylene dioxythiophene):poly(styrene sulfonate) (PEDOT:PSS) layer can be spin coated as buffer layer on ITO, between the anode and photoactive layer to prevent photoactive layer from oxidation besides its advantages such as an exciton blocker and smoothing the ITO surface (Jia et al., 2016). The photoactive layer absorbing light contains polymer donor and inorganic acceptor materials. Although aluminum, gold and silver usually are used for the cathode, sometimes magnesium and calcium are used. The task of the cathode electrode is gathering electrons from the device. The device produced is illuminated by ITO or FTO.

OPV devices work differently than that of silicon ones since the organic semiconductors' elemental characteristics are different from that of inorganic equivalents. Low relative dielectric constant of organic semiconductors ($\varepsilon_r = \sim 3$) leads to a large electrostatic force between holes and electrons, an excited state –where hole and electron are coulombically bound– is created after the photoactive layer is hit by light and the electron–hole pair that is coulombically bound is called as exciton. The production and transportation of free charge carriers throughout the device are observed after a force broke the excitonic binding energy. The excitons that are created in the donor material are separated at the donor–acceptor (D–A) interface in HSCs. The conduction band edge of the acceptor materials and the energy level offset of the lowest unoccupied molecular orbital (LUMO) of the donor presents the force that is needed to break this exciton binding energy. Excited state energy offset is referred to energy offset used to separate excitons. In the acceptor material, the valence band edge of the acceptor materials and the energy offset of the highest occupied molecular orbital (HOMO) of the donor presents the force that is needed to break the exciton binding energy for exciton separation. This energy offset used to separate excitons is referred to ground state energy offset (Pan, 2009). To obtain a successfully operating device, it is crucial to arrange both materials in the active layer whilst separation of exciton takes place at the interface of D–A phase due to this energy offset. In bi–layer structures, excitonic separation is inadequate due to the small excitonic diffusion length in conjugated polymers (~ 10 nm) since only one interface exists. Free charge carriers can only be produced by photoexcitation that occurs within an excitonic diffusion length of the interface since the single interface between the

materials is the only place where separation can occur. Excitonic separation, as a result of interfacial area increment, can be increased by mixing the donor and acceptor materials and this new device structure formed is called bulk heterojunction. The both heterojunction device structures mentioned are shown in Fig. 1.1. A device with a large dispersion of interfaces throughout the photoactive layer necessitates smaller exciton diffusion distances; hence, a larger exciton dissociation yield is succeded. Increasing the interfacial area causes a decrease in the creation of efficient conductive pathways. Thus, it is crucial to arrange the donor and acceptor phases for the device performance (Töreli, 2018).

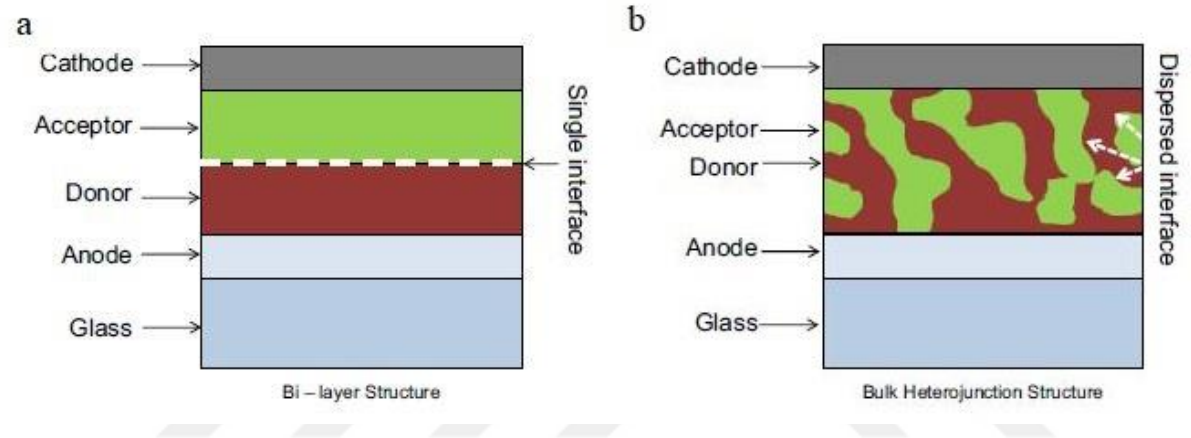

Figure 1.1. Schematic diagram of (a) bi–layer, and (b) bulk heterojunctions photoactive layer (Wright & Uddin, 2012).

The formation of an exciton is observed when the donor material absorbs an electron, and this exciton is separated as electrons and holes on the D–A interface, as it is already mentioned above. As a result of separation, the electron is transferred to the acceptor material at the interface and then the electron is transferred to the cathode for accumulation of the charges. The hole formed in the donor material is transferred across the polymer and gathered at the anode. This process is as shown in the Fig. 1.2 (a). Inorganic acceptor can also benefit for useful photocurrent. The exciton formed via absorption of the light by acceptor material decomposes to the HOMO energy level and acceptor valence band edge. After the transmission process of holes to the donor material at the interface is carried out, the hole is transported to the anode. Meanwhile, the electron moves to the cathode after it remains in the acceptor material. This process is illustrated in Fig. 1.2 (b) (Wright & Uddin, 2012).

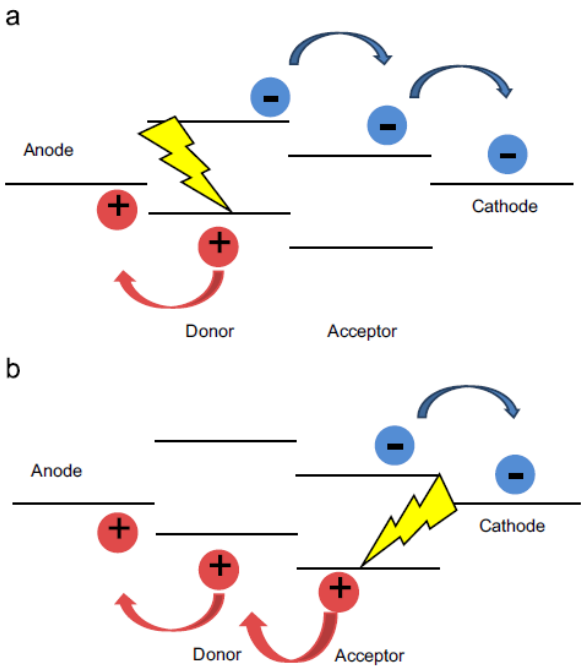

Figure 1.2. Schematic representation of charge transfer, (a) photo production in electron donor, (b) photo production in electron acceptor (Wright & Uddin, 2012).

1.2.1. Power conversion efficiency (PCE, Ƞ)

The PCE of a SC is defined as:

$$PCE = \frac{J_{sc}\ x\ V_{oc}\ x\ \mathrm{FF}}{P_{in}} \tag{1}$$

where J_{sc} is short circuit current density, V_{oc} is open circuit voltage, FF is fill factor and P_{in} is incident input power. An international standard input power of AM 1.5 G, with an intensity of 100 mW/cm^2 while the cell is at room temperature (RT), is applied to device to determine the performance. Thus, the major factors that influence PCE of HSCs are J_{sc}, V_{oc} and FF and they are explained below. In addition, these characteristics are illustrated in Fig. 1.3 as a typical illuminated J–V characteristic.

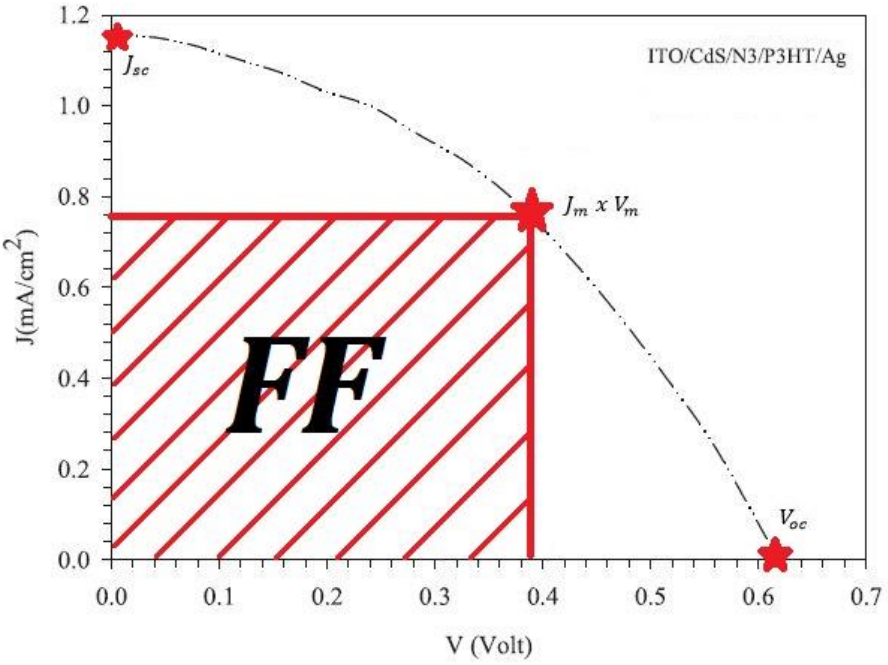

Figure 1.3. Current density–voltage (J–V) characteristics of ITO/CdS/N3/P3HT/Ag structure, indicating the three major device characteristics that determine efficiency (Yılmaz, Ünverdi, Tomakin, Polat, & Bacaksız, 2019).

1.2.2. Short circuit current density (J_{sc})

The short circuit current density, J_{sc} can be obtained when the device is at short circuit conditions, and is defined as the maximum photocurrent density, which is directly associated with external quantum efficiency, EQE. This relationship is shown below as:

$$J_{sc} = \frac{q}{\hbar c}\int_{\lambda_{min}}^{\lambda_{max}} EQE\ x\ P_{in}(\lambda)\lambda\ x\ dx \tag{2}$$

At a specific wavelength, EQE is obtained by dividing the photo–generated electrons collected to the number of incident photons. This quantity depends on five major steps whose each have some impacts on the efficiency of a HSC. Thus, EQE can be expressed as:

$$EQE = \eta_{abs}\ x\ \eta_{diff}\ x\ \eta_{diss}\ x\ \eta_{tr}\ x\ \eta_{cc} \tag{3}$$

where η_{abs} is the absorption yield of the device, η_{diff} is the ability of an exciton to diffuse to a D–A interface, η_{diss} is the exciton dissociation yield, η_{tr} is the efficiency of charge carrier transport throughout the device and η_{cc} is the efficiency of charge collection at the electrodes.

1.2.3. Open circuit voltage (*Voc*)

Open circuit voltage describes the voltage at which current is zero through the external circuit and is defined as:

$$V_{oc} = \frac{k_B T}{q} \ln\left(\frac{J_{ph}}{J_0} + 1\right) \tag{4}$$

where k_B is Boltzmann constant, T is temperature, q is charge, J_{ph} is photo–generated current density and J_0 is saturation current density. The maximum voltage obtained from a SC is defined as open circuit voltage. It depends on both the photo–generated current and saturation current density, as it is seen from the formula above. The saturation current density has more influence than J_{ph} on V_{oc} since the alteration of J_0 is by orders of magnitude. V_{oc} is a measure of the amount of recombinations in the SC since the saturation current density relies upon recombination.

1.2.4. Fill factor (*FF*)

The proportion of the maximum power ($P_{max} = J_m x V_m$) produced by a SC and the product of V_{oc} by J_{sc} is described as fill factor, implying that it is the squareness of the J–V curve, and is defined as:

$$Fill\ Factor = \frac{J_m\ x\ V_m}{J_{sc}\ x\ V_{oc}} \tag{5}$$

where J_m and V_m are the maximum power current density and voltage, respectively, J_{sc} is the short circuit current density and V_{oc} is the open circuit voltage. Fill factor is limited practically and is less than 1 (ideal value) due to the existence of physical restraints on diode quality. A real diode will behave differently than that of ideal one due to the recombination that occurs at junction. The junction is at the D–A interface for both OPV and organic–inorganic HSCs.

The parasitic loss mechanisms of shunt and series resistance can alter the aspect of the J–V curve quantitatively that caused by the diversion from the ideal case. In ideal case, the series resistance is zero ($R_s = 0$), however, the enhanced series resistance is obtained via weak conductivity through the active layer and reduced charge carrier injection to the electrodes. The infinite shunt resistance ($R_{sh} = \infty$) is required for the ideal diode by contrast to series resistance. The current leakage and imperfections within the photoactive film leads to a decrement in shunt resistance of the device.

1.3. Aim of Study

CdS was used as the inorganic semiconductor material and P3HT was used as the organic semiconductor polymer for HSCs to be produced. CdS is one of the II–VI group with a direct transited semiconductor materials and has a good chemical stability as well as an n–type conductivity. Compared to other semiconductors (ZnO and TiO_2), the forbidden energy bandwidth is 2.42 eV at RT that makes it more suitable for photovoltaic applications. In addition, having a good electron acceptor material makes CdS one of the most promising photoactive materials. As an electron donor material, p–type semiconductor P3HT [poly(3-hexylthiophene-2,5-diyl)] polymer was chosen due to its large hole mobility and fast charge transfer. The difference between the LUMO and HOMO energy levels of the P3HT polymer is 1.9 eV, which allows it to be used as a material with a wide absorption spectrum in HSCs. In addition, P3HT semiconductor polymer is one of the best p–type conductivity materials that can be kept in dark conditions by virtue of light–stable structure. Due to these properties, the use of P3HT as an organic material has become attractive recently. However, one of the most known disadvantages of organic materials is their reduced stability compared to inorganic materials. Therefore, the organic and hybrid–based SCs produced today are not a part of PV market due to the common occurrence of degradation of organic materials. As known from the literature studies, the stability of SCs produced on both organic and hybrid basis is weak, and hence the PCE of the produced SC decreases to half of its original value and even less than half in a few months or a few days. This is an obstacle to the active use of organic and hybrid–based SCs in today's world.

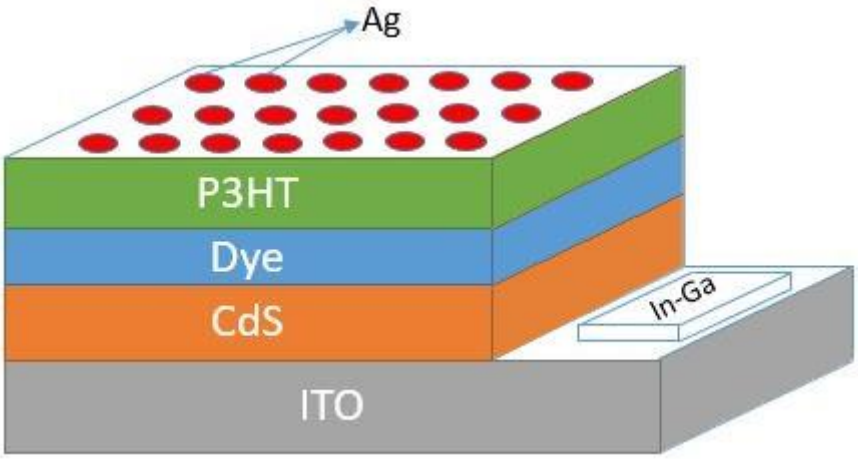

Figure 1.4. Schematic representation of the CdS based hybrid solar cells planned to be produced.

In this study, ITO was used as an anode electrode of CdS/P3HT HSCs and Ag was used as the cathode electrode. The schematic representation of the HSCs is shown above (Fig. 1.4) and the effects of various sorts of dyes (Eosin–Y, D205, N719 and N3) and different morphologies of CdS samples grown by spray pyrolysis, chemical bath deposition, doctor blade and hydrothermal method on the HSC efficiency were investigated. For this, dye coatings such as Eosin–Y (organic dye), D205 (indolin dye), N719 (Ru–based complex dye) and N3 (Ru–based complex dye) were applied on CdS samples that are in different morphologies and were coated on ITO before P3HT coating was carried out by a spin coater. Thus, ITO/CdS thin film/dye/P3HT/Ag, ITO/CdS paste/dye/P3HT/Ag and ITO/CdS nanosphere/dye/P3HT/Ag HSCs were fabricated. The influences of diverse dyes on CdS samples produced in different morphologies were evaluated in terms of structural, morphological and optical measurements for the first time as known from literature survey. In addition, SC parameters of photovoltaic devices obtained from CdS samples produced in different morphologies and covered with different dyes were determined.

2. LITERATURE REVIEW

The literature review made in this work consists of two steps. The first step includes HSCs produced by CdS or ZnO or TiO_2 samples with different morphologies obtained by different methods. In the second step, it is related to studies examining the effects of dye modification of the surfaces of CdS or ZnO or TiO_2 samples produced in different morphologies on the efficiency of SCs.

According to the literature review, it is seen that although the number of studies on ZnO and TiO_2 based HSCs with different morphologies is sufficient, the density of papers on CdS–based ones are scarce. For example, Ruankham, Yoshikawa and Sagawa (2013) fabricated ZnO nanorods and nanoparticles on ITO by spin–coating/hydrothermal and precipitation method, respectively to form ZnO/P3HT HSCs. The PCEs of ZnO nanorods and nanoparticles–based devices were found as 0.259% and 0.205%, respectively. Urgessa, Ruess, Tankio Djiokap, Botha and Schlettwein (2019) produced ZnO nanorods, nanorods–nanoparticles on FTO through chemical bath deposition, and a two–step solution based method, respectively. The influence of morphology on the efficiency of ZnO nanorods based-dye sensitized solar cells (DSSCs) was investigated. PCEs of 0.8% and 0.697% were found for bare ZnO nanorods and hybrid ZnO nanorods–nanoparticles, respectively. PEDOT: PSS was covered on ITO as a buffer layer by Jia et al. (2016) to fabricate ITO/PEDOT:PSS/P3HT/ZnO/Al HSCs. Subsequently, the liquid crystal molecules of DPP–TP6 was added into the P3HT/ZnO HSCs to produce ITO/PEDOT:PSS/P3HT/ZnO/DPP–TP6/Al SCs for the investigation of morphology effect. An increase in the PCE values of ZnO HSCs was observed and the efficiency with and without DPP–TP6 (15%) were reported as 0.54% and 0.26%, respectively. Ishwara (2017) synthesized multi (ITO/compact TiO_2/nanoporous TiO_2/P3HT/PEDOT:PSS/Au) and bi–layer (ITO/compact TiO_2/P3HT/ PEDOT:PSS/Au) TiO_2/P3HT HSCs by spray pyrolysis and spin–coating techniques to study the morphology effects on the power conversion efficiency values and he found different efficiency values for both devices. Bozkurt Çırak et al. (2020) synthesized TiO_2 nanotubes on titanium foils by anodic oxidation to form titanium dioxide nanotube array (TNA). After TNAs were obtained, they produced ZnO nanorods on the surface of TNAs through hydrothermal method. The effects of morphology and growth temperature on the PCE of

DSSCs were investigated. It was found that PCE values increased upon ZnO deposition and the increasing temperature, and efficiency was obtained up to more than twofold compared to that of pristine one. Various studies on the morphology effects of CdS–based SCs on the PCE are as follows: Chen et al. (2011) obtained CdS nanorods on ITO in two steps by electrodeposition and hydrothermal method, respectively. They fabricated the ITO/CdS/MEH–PPV/Au heterostructure by depositing the polymeric material named MEH–PPV on the formed CdS nanorods. The maximum SC efficiency obtained for this structure is 0.06%. Aydin Yüksel, Güneş and Güney (2013) grew CdS thin films on ITO via spray pyrolysis technique. P3HT organic material was covered by drop–cast method on the films and after Au evaporation, ITO/CdS/P3HT/Au SC was attained. SC efficiency was calculated as 0.15%. CdS thin films on ITO were grown by Arenas, Mendoza, Cortina, Nicho and Hu (2010) by CBD route. P3OT polymer material was coated on CdS thin films to obtain ITO/CdS/P3OT/Au heterostructure. The PCE of the produced SC was found to be 0.06%. Deng and Chen (2013) produced the CdS nanorods on ITO by hydrothermal method. They coated the PCPDTBSe semiconductor polymer material on the CdS samples to prepare ITO/CdS nanorods/PCPDTBSe/Au HSCs. They found that the maximum efficiency of the cell was 0.10%. CdS thin films by CBD were obtained by Zhu et al. (2012) on ITO. They investigated the effects of CdS thin film growth time and duration on the PCE of CdS–based HSCs. The highest PCE of the produced ITO/CdS/P3HT: PCBM/MoO3/Au heterostructure was 1.42% at a growth temperature of 50 ℃ and 60 minutes of growth time. Yang, Li, Zhang and Li (2013) produced FTO/CdS/P3HT/Au SCs by synthesizing multi–branched CdS nanorods in two steps via hydrothermal method on FTO. They calculated the efficiency of the obtained SC as 0.25%. Jabeen et al. (2017) produced CdS nanowires by three steps on PEDOT–PSS coated ITO. They used P3HT as the polymeric semiconductor material and Al as the cathode electrode. Thus, they fabricated ITO/PEDOT:PSS/CdS/P3HT/Al SC and found its efficiency as 0.30%. As can be seen from the studies discussed above, the efficiency values of HSCs obtained by produced CdS or ZnO or TiO_2 samples in different morphologies by different methods are also different.

Although the number of studies on CdS–based HSCs that have been surface–modified via different dyes is limited, the amount of the reported studies based on TiO_2 and ZnO is plenty in the literature. For example, Urgessa et al. (2019) fabricated ZnO nanorods on FTO by a two–step solution method. They investigated the impact of surface modification on the

performance of ZnO nanorods DSSCs, and an increase in the PCE of ZnO nanorods modified with Eosin–Y and DN216 dyes were reported. Yun-Yue Lin et al. (2009) examined the effects of ACA, CuPc, N3 dyes on ITO/PEDOT:PSS/P3HT:TiO_2/dye/TiO_2/Al SCs. Increases in the PCE of SCs with dye coatings have been recorded. Ruankham, Macaraig, Sagawa, Nakazumi and Yoshikawa (2011) studied the impact of surface alteration of ZnO nanorods by small organic molecular dyes on polymer–inorganic HSCs. They fabricated ZnO nanorods on ITO. The surface modification of ZnO nanorods was carried out by different (NKX2667, N719, D205, Sq) dyes. They observed an increment in the PCEs of ZnO nanorods upon surface modification. In addition, they investigated absorption conditions such as soaking time and temperature. The best PCE values were observed for 60 minutes at 60 ℃. TiO_2 nanorod arrays (NRAs) were prepared through hydrothermal route on FTO by Pei et al. (2016) to obtain FTO/TiO_2 NRAs/modifier/P3HT/PEDOT:PSS/Au SC. Triphenylamine dye was used as interfacial modifier and Zonyl FS 300 was used as surfactant for PEDOT:PSS to get rid of the incompatibility between P3HT and PEDOT:PSS. After interfacial modification with triphenylamine dye, approximately a tenfold efficiency value (2.01%) of that pristine (0.21%) one was reported. Lim, Yap, Yahaya and Salleh (2013) grew ZnO nanorods by hydrothermal method on FTO. The surface of the ZnO nanorods was modified with the Eosin–Y dye having different concentrations, and FTO/ZnO/Eosin–Y/P3HT/Ag HSCs were produced. It was found that PCE was increased from 0.05% to 0.39% with dye coating. ZnO NRAs on transparent conducting oxide (TCO) coated glass pieces were fabricated by P. Zhong et al. (2014) via liquid phase epitaxial growth method. Interfacial modification of P3HT/ZnO NRAs was made by third components (N719 dye and CdS). They obtained a threefold enhancement in the PCE of ZnO NRAs with surface modification of N719 dye from 0.034% to 0.136%. As already mentioned above, there are limited number of studies on surface modification of CdS samples via different dyes. For example, after forming a thin TiO_2 layer on FTO, M. Zhong et al. (2012) produced the FTO/TiO_2/CdS/N719 dye/P3HT/Au HSC by coating the CdS nanoparticles onto this formed structure using the doctor blade technique. They calculated PCEs of CdS samples as 0.06% and 1.06% before and after surface modification via N719 dye, respectively. Nan et al. (2013) synthesized CdS nanorods on ITO with the help of hydrothermal method. The N719 dye was coated on the obtained CdS samples to produce ITO/CdS/N719 dye/P3HT/Au SC. The PCE of the HSC was determined to be 0.24%. Furthermore, the efficiency of SCs without N719 dye coating was found to be 0.03%. Jabeen et al. (2017) obtained CdS nanowire–based HSCs on PEDOT:PSS coated ITO.

They covered the “Porphyrin” dye on CdS nanowire surfaces and examined the effects of different concentrations of dye on PCE. While the PCE value of the SC (ITO/PEDOT:PSS/CdS/polyphyrin/Al) without dye coating was obtained as 0.30%, the highest efficiency value after the dye coating was calculated as 0.50%. It is seen from the literature studies discussed above that the surface modification of semiconductor materials improves the PCE of the produced HSCs. This improvement is due to increased charge dissociation efficiency at the CdS/P3HT interface. That is, with the improvement of exciton separation between the CdS and P3HT layers, interface charge recombination decreases, thereby both open circuit voltage (V_{oc}) and short circuit current (I_{sc}) increase.

In this work, CdS samples were grown on ITO in different morphologies using different methods. CdS thin films were fabricated by spray pyrolysis and chemical bath deposition methods. On the other hand, hydrothermal method was utilized to obtain nanosphere morphology after forming a thin CdS seed layer via chemical bath route. The P3HT semiconductor polymer was coated on CdS samples with different morphologies by spin–coating method. Finally, using element Ag as a cathode electrode, ITO/CdS/P3HT/Ag HSCs were produced. Besides different morphology effects, ITO/CdS/dye/P3HT/Ag HSCs were produced making surface modification of CdS samples with different dyes (Eosin–Y, D205, N719 and N3). Thus, alterations in the PCE values of the HSCs produced with CdS samples both with different morphologies and exposed to different dyes were investigated for the first time as known from literature survey.

3. MATERIALS AND METHODS

3.1. Spray Pyrolysis Method

Spray pyrolysis method is defined as a method to form thin films on the substrate as a result of chemical reactions. In this method, the solution is prepared by adding salts of specific concentrations containing the elements of the material desired to be produced. After the solution has been prepared, this solution is sprayed onto the preheated substrates in a certain time and flow rate as fine droplets. In the spraying process, nitrogen gas or air is used as the carrier gas. Thin film quality and its properties significantly depend on spray parameters. Substrate temperature, solution flow rate, type of salts used, type of solvent, spray time, distance between nozzle–substrate, angle of spray head, etc. are examples of these. Many properties of the materials to be produced such as thickness, electrical and optical properties can be changed by controlling these parameters (Perednis & Gauckler, 2005).

The most important advantages of spray pyrolysis method are low cost, simplicity in thin film production, covering large areas and obtaining very homogeneous thin films. The schematic diagram showing the spray pyrolysis set-up to be used is given in Figure 3.1.

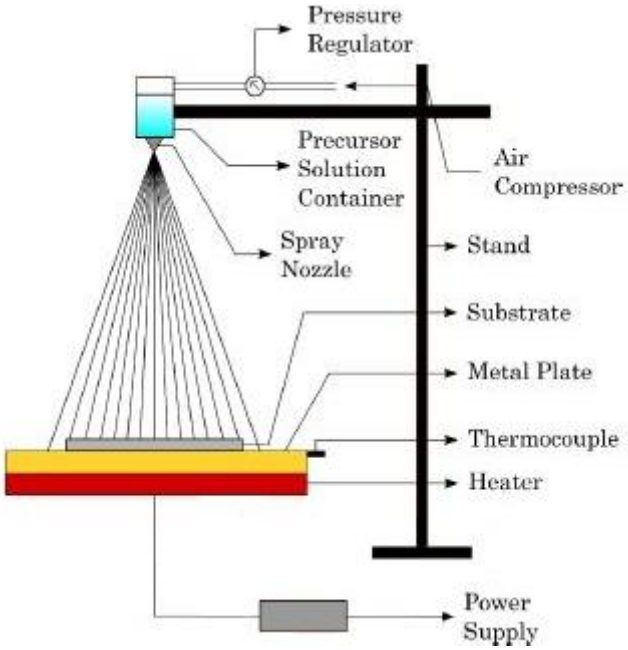

Figure 3.1. Schematic representation of the spray pyrolysis method.

3.2. Production of CdS Thin Films by Spray Pyrolysis Method

CdS thin films were produced on 1x1.25 cm^2 sized ITO by spray pyrolysis technique. $CdCl_2$ was used as the cadmium source whereas thiourea ($(NH_2)_2CS$) chemical salt was employed as the sulfur source. The substrates were in turn cleaned by acetone, ethanol and deionized water in an ultrasonic bath for 10 minutes, and they were rinsed by deionized water for avoiding of unwanted substances and drying process was carried out by flowing air. In the production of CdS thin films, solutions of 0.05 M and 0.1 M concentrations of $CdCl_2$ and ($(NH_2)_2CS$) salts dissolved in deionized water were utilized. The pH of the solution was measured as 6.5. The prepared mixture was sprayed on ITO for 10 minutes with the help of compressed air at a temperature of 400 °C. The distance between the substrates and the nozzle (spray head) was 20 cm and the spray rate was set to 2 ml/min. In addition, the substrates were rotated at a speed of 10 rpm using a constant speed step motor during spraying to produce films homogeneously. After spraying was completed, the samples were taken onto Al_2O_3 plates and cooled quickly to prevent oxidation of the samples. After the growth was completed, it was observed that the samples were homogeneously coated and adherence between CdS films and ITO were good (Figure 3.2).

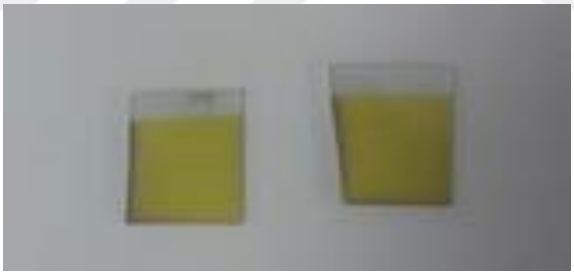

Figure 3.2. CdS thin films grown by spray pyrolysis on ITO coated glass substrates.

3.3. Chemical Bath Deposition (CBD) Method

The chemical bath deposition method is one of the solution–based methods and is frequently used to obtain semiconductor compounds from aqueous solutions. With this method, homogeneous and well adhesioned–films can be formed on the appropriate substrates by controlled deposition of the compounds from the prepared solution. Compared to vapor phase synthetic methods, this method has many advantages. Also, it allows us to easily control thin film growth parameters such as film thickness, precipitation rate, varying solution pH value, quality of crystallites, temperature and solution concentration (Adaikalam et al., 2010). It is a cheap method that does not require high voltage and can be employed at RT. The most

important requirements are a solution containing the salts of the compound to be formed and a substrate on which the film will be grown. However, this method has some concerns about reproducible results compared to other chemical methods. However, with proper and careful optimization, reasonable results can be easily achieved. Figure 3.3 shows the chemical bath deposition system we use to grow CdS thin films in our laboratory.

Figure 3.3. Chemical bath deposition system used to produce CdS thin film.

3.4. Production of CdS Thin Films by CBD Method

ITOs were subjected to the same cutting and cleaning process mentioned above. The solution prepared to grow CdS thin films via chemical bath deposition method contains $CdCl_2$, thiourea, NH_4Cl and NH_4OH chemicals. Each chemical material was dissolved separately in deionized water as 0.02 M $CdCl_2$, 0.05 M thiourea, 0.05 M NH_4Cl. Then, the solutions were transferred to the beaker for coating process. A suitable amount of NH_4OH was added to the mixture so that the pH of the formed solution was 11. The cleaned ITO were immersed in the solution and started to be heated from RT and reached 75 ℃ in about 3 hours and kept at this temperature for 15 minutes. As a result of this period, the samples were removed from the

solution and rinsed with distilled water various times to get rid of the undesired residual layer. The surface adhesion of CdS thin films obtained on ITO was found to be good (Figure 3.4).

Figure 3.4. CdS thin films grown by chemical bath deposition on ITO coated glass substrates.

3.5. Production of CdS Powders by CBD and Doctor Blade Method

The procedure applied to obtain CdS thin films by above–mentioned CBD method was repeated to obtain CdS powder samples. Differently, no ITO were placed in the solution and the water in the solution was evaporated by waiting for a long time at a temperature of 75 ℃. The powders obtained were subjected to cleaning/washing with pure water several times to remove unwanted substances and then drying at 75 ℃. The appearance of the powders obtained is shown in Figure 3.5 (a).

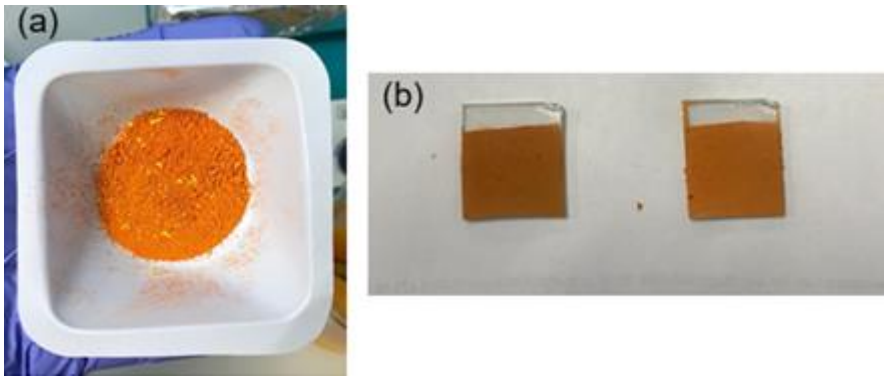

Figure 3.5. (a) CdS powder sample, (b) CdS paste samples obtained on ITO coated glass substrates by a doctor blade method.

In order to use CdS powders in a SC application, a mixture was obtained for coating on ITO. The resulting mixture was formed from 2 g CdS powder, 4 ml distilled water, 10 µl acetylacetone and 50 µl triton (TX–100) chemicals. The obtained viscous paste was coated on ITO by virtue of doctor blade method and the samples obtained were annealed at 350 ℃ for

30 minutes in the air and vaporized from unwanted organic components. The photograph of the CdS paste sample obtained at the end of these processes and coated on ITO is given in Figure 3.5 (b).

3.6. Hydrothermal Method

The hydrothermal method is one of the most popular techniques used to grow nanostructured materials. This method has attracted a lot of attention of scientists' over the past 15 years. The word "hydrothermal" has a geological origin; the word "hydro" means water, while the word "thermal" means heat. The term hydrothermal refers to heterogeneous reactions occurring in a liquid solution under high pressure and temperature. In hydrothermal method, water is generally used as solvent. The water exposed to hydrothermal conditions exhibits different features than that of standard state. The reason for using water as a solvent is that it is low cost and environmentally friendly. In addition, due to being fireproof and volatile, non–toxic and thermodynamically stable, water often is used in this method. Hydrothermal system consists of autoclave, beaker, heater, thermometer and digital indicator. For material synthesis, a container called autoclave made of stainless steel is utilized. Generally teflon is employed as beaker. The beaker must be fully inserted into the autoclave without leaving any gaps. Compared to other advanced material growth techniques, the hydrothermal method is highly preferred because of the cheap device prices and use of less energy. Moreover, it is an environmentally friendly method. Variations that may occur in morphology and particle size can be achieved by this method (Bozkurt Çırak et al., 2020). Figure 3.6 shows the hydrothermal system we use to grow CdS nanospheres in our laboratory.

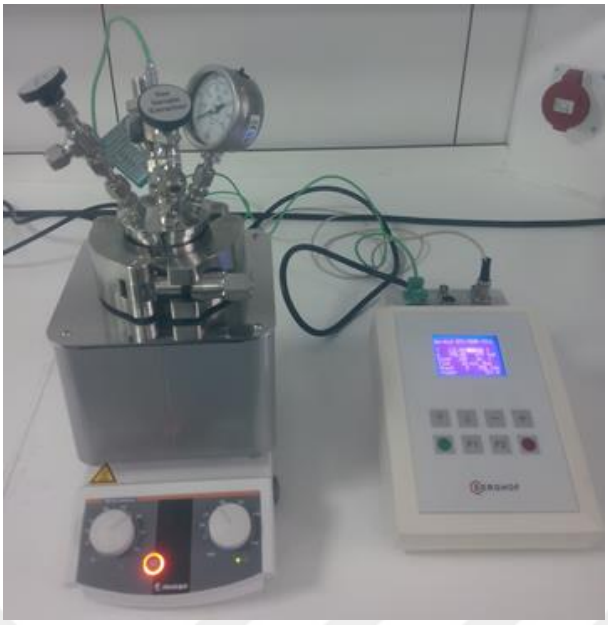

Figure 3.6. Hydrothermal system used to produce CdS nanospheres.

3.7. Production of CdS Nanospheres by Hydrothermal Method

CdS nanospheres were obtained in two steps. First of all, CdS seed layer was grown on ITO by using CBD method. The growth process of the CdS seed layer is exactly the same as producing CdS thin films obtained by the CBD method above. CdS nanospheres were obtained by using hydrothermal method on CdS seed layer. ITO were cleaned with the help of sulfuric acid, pure water and ethanol in the ultrasonic bath for 10 minutes, respectively and subsequently the substrate surfaces were dried with nitrogen gas. To produce CdS nanospheres, cadmium nitrate tetrahydrate ($Cd(NO_3)_2.4H_2O$) was used as a source of cadmium; thiourea ($(NH_2)_2CS$) as a source of sulfur; and glutathione as a reducing agent. Cd/S/glutathione molar ratio in solution was chosen as 1:3:0.6. 1.11 g cadmium nitrate, 0.82 g thiourea and 0.66 g glutathione chemicals were dissolved separately in 20 ml of distilled water and three different solutions were poured into teflon container and distilled water was added to the prepared solution in order to complete 75 ml. The Teflon container was placed inside the autoclave made of stainless steel and the autoclave was closed by placing the uncut–substrates vertically inside the teflon container. The temperature of the solution was heated to 150 ℃ by the temperature controller and at this temperature, it was waited for 3.5 hours to grow CdS nanospheres. After growth process, the teflon container was allowed to cool down to the RT, and the samples were taken out, rinsed with deionized water, and

subsequently the samples were dried by nitrogen gas. The photography of CdS nanospheres grown on the CdS seed layer is shown in Figure 3.7.

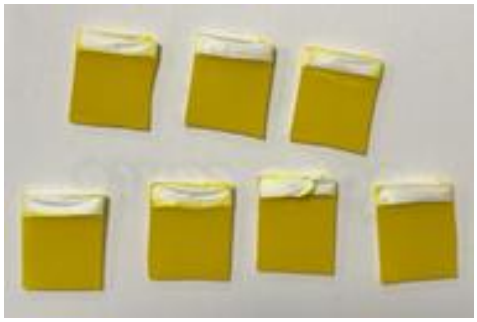

Figure 3.7. CdS nanospheres grown by two steps on ITO coated glass substrates.

3.8. Surface Modification of CdS Samples via Diverse Dyes

Eosin–Y dye: 5 mM Eosin–Y dye stuff was dissolved in acetone to prepare the desired solution and an orange solution in color was obtained (Figure 3.8 (a)). CdS samples grown on ITO with different methods were first soaked in the dye solution for 24 hours. As a result of not enough coating, additional dye coating was applied to the CdS samples with a spin–coating device as 20 times at a speed of 1000 rpm, with one–minute coating time for each. Photographs of samples with Eosin–Y dye coatings are given in Figure 3.8 (b)–(e). It appeared that the adhesion of Eosin–Y dye stuff on the CdS thin film surface produced by spray pyrolysis was much weaker than those of the others.

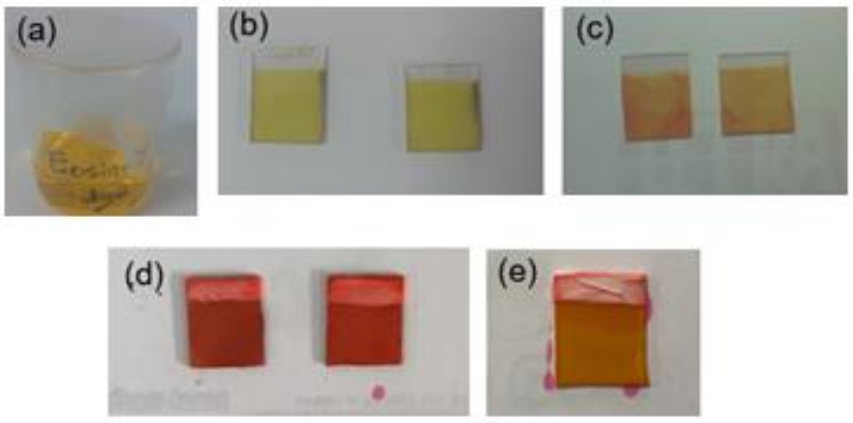

Figure 3.8. (a) Eosin–Y dye solution, (b) CdS thin films produced by spray pyrolysis method and coated with Eosin–Y dye, (c) CdS thin films produced by chemical bath deposition and coated with Eosin–Y dye, (d) CdS paste coated with Eosin–Y dye, (e) CdS nanosphere coated with Eosin–Y dye.

D205 dye: D205 dye with a concentration of 0.3 mM dissolved in solution containing acetonitrile and tert–butyl alcohol (1:1) (Figure 3.9 (a)). CdS thin films were kept in the obtained dye solution for 24 hours. Additionally, dye solution was also applied to the surface of the CdS samples with a spin–coating device with a spinning speed of 1500 rpm for 10 times and one minute for each. Photographs of the coated samples are given in Figure 3.9 (b)–(e). D205 dye stuff adhesion on the surface of CdS samples grown with different methods was found to be good.

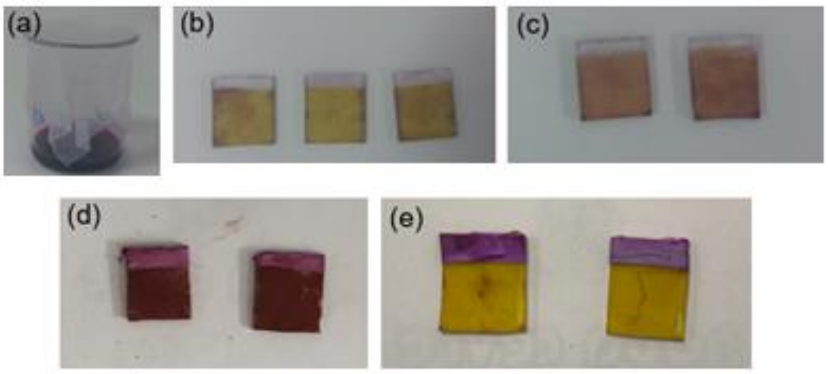

Figure 3.9. (a) D205 dye solution, (b) CdS thin films produced by spray pyrolysis method and coated with D205 dye, (c) CdS thin films produced by chemical bath deposition and coated with D205 dye, (d) CdS paste coated with D205 dye, (e) CdS nanosphere coated with D205 dye.

N3 dye: After dissolving 0.5 mM N3 dye in pure ethanol, the samples were kept in this solution for 24 hours and hence, N3 dye coating was performed (Figure 3.10 (a)). However, as a result of lack of dye coating, additional dye coating was applied to the surface of CdS samples by spin–coating method for 15 times at a spinning speed of 1000 rpm, one minute for each. Photographs of CdS samples with N3 dye coatings were given in Figure 3.10 (b)–(e). It was determined that the adhesion of N3 dye stuff was weaker on the surface of CdS thin films produced by spray pyrolysis than those of the others.

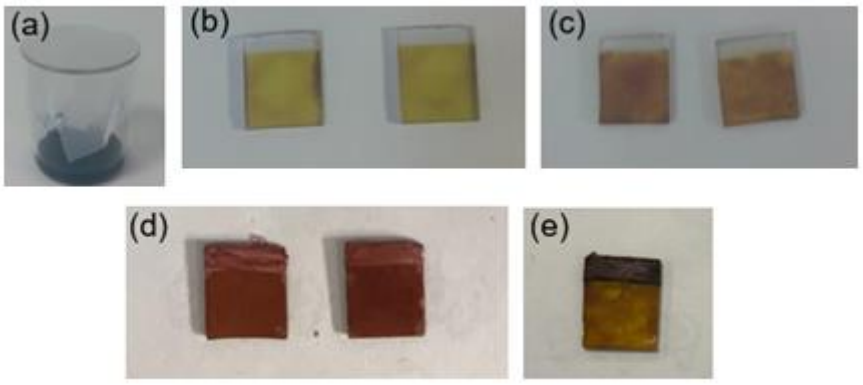

Figure 3.10. (a) N3 dye solution, (b) CdS thin films produced by spray pyrolysis method and coated with N3 dye, (c) CdS thin films produced by chemical bath deposition and coated with N3 dye, (d) CdS paste coated with N3 dye, (e) CdS nanosphere coated with N3 dye.

N719 dye: 0.5 mM N719 dye was dissolved in pure ethanol to obtain the desired solution (Figure 3.11 (a)). CdS samples grown on ITO were kept in this solution for 24 hours, however it was found that there was not enough coating on the surface. Thus, the additional coating process was carried out for the surface of the CdS samples as 10 times at a spinning speed of 1000 rpm, one minute for each with the spin–coating device. The results obtained are presented in Figure 3.11 (b)–(e). The weakest N719 dye coating was found to occur for samples grown by spray pyrolysis.

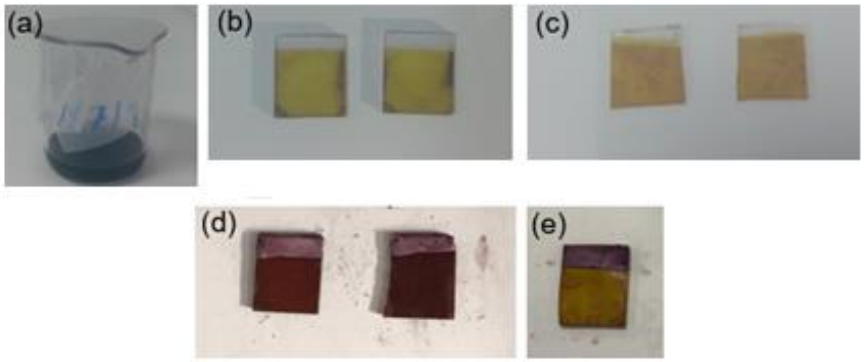

Figure 3.11. (a) N719 dye solution, (b) CdS thin films produced by spray pyrolysis method and coated with N719 dye, (c) CdS thin films produced by chemical bath deposition and coated with N719 dye, (d) CdS paste coated with N719 dye, (e) CdS nanosphere coated with N719 dye.

3.9. Coating of P3HT Material on CdS Samples Grown by Different Methods

20 mg/ml of commercial P3HT material was dissolved in 2 ml of chlorobenzene (Figure 3.12 (a)). P3HT solution was then applied on CdS samples, which were grown on ITO by different methods, with and without dye, with the help of a spin–coater, at a spinning rate of 1000 rpm, for 5 times, one minute for each period. Figure 3.12 (b) shows the P3HT organic material coated on ITO. Figure 3.12 (c) indicates the ITO/CdS thin film (spray)/P3HT sandwich structure and Figure 3.12 (d) shows the ITO/CdS thin film (CBD)/D205 dye/P3HT heterostructure. On the other hand, ITO/CdS paste/Eosin–Y dye/P3HT and ITO/CdS nanosphere/P3HT heterostructures are shown in Figure 3.12 (e) and (f), respectively. According to the results obtained from each photographs as displayed in Figure 3.12 (b)-(f), P3HT organic material can be easily coated on both the ITO and on the CdS surfaces with and without dye.

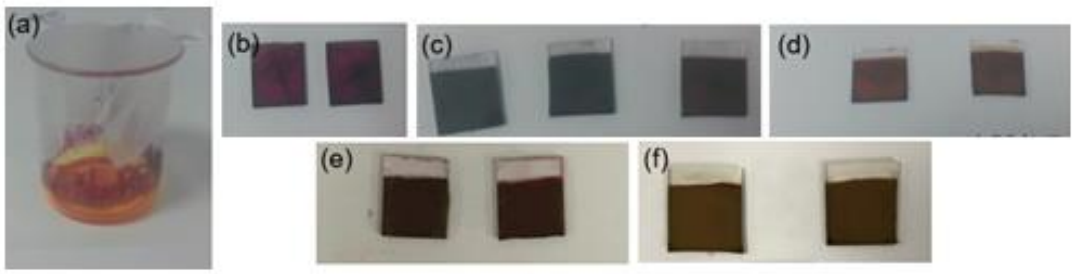

Figure 3.12. (a) P3HT solution, (b) P3HT film coated on ITO coated glass substrates, (c) ITO/CdS thin film (spray)/P3HT sandwiched structure, (d) ITO/CdS thin film (CBD)/D205 dye/P3HT heterostructure, (e) ITO/CdS paste/Eosin–Y dye/P3HT and (f) ITO/CdS nanosphere/P3HT heterostructure.

3.10. Fabrication of CdS–based Hybrid Solar Cells

CdS–based HSCs were completed by depositing Ag paste as front contact with a contact area of 0.008 cm^2 on these heterostructures. As a back contact, “In-Ga” alloy was used. Figure 3.13 (a)–(d) show photographs of ITO/CdS thin film (spray)/P3HT/Ag, ITO/CdS thin film (CBD)/D205 dye/P3HT/Ag, ITO/CdS paste/N719 dye/P3HT/Ag and ITO/CdS nanosphere/Eosin–Y dye/P3HT/Ag HSCs, respectively.

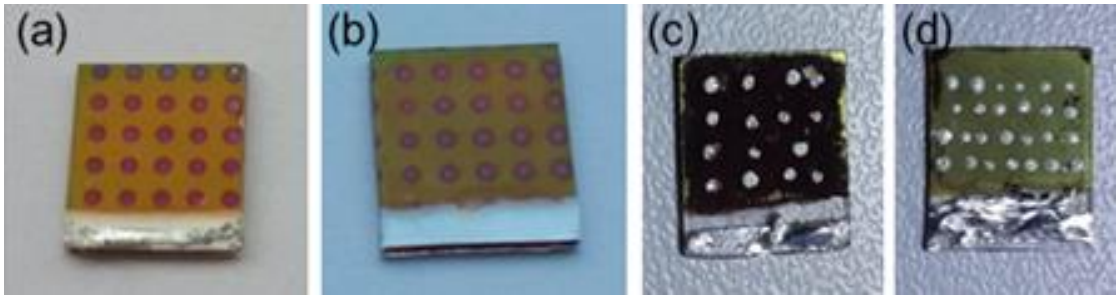

Figure 3.13. Hybrid solar cells of (a) ITO/CdS thin film (spray)/P3HT/Ag, (b) ITO/CdS thin film (CBD)/D205 dye/P3HT/Ag, (c)ITO/CdS paste/N719 dye/P3HT/Ag, and (d) ITO/CdS nanosphere/Eosin–Y dye/P3HT/Ag.

Table 3.1. Codes, names and synthesis methods of produced CdS based samples.

Sample Code	Sample Name	Synthesis Method
A0	ITO/CdS thin film	Spray Pyrolysis
A1	ITO/CdS thin film/P3HT/Ag	Spray Pyrolysis
A2	ITO/CdS thin film/Eosin–Y/P3HT/Ag	Spray Pyrolysis
A3	ITO/CdS thin film/D205/P3HT/Ag	Spray Pyrolysis
A4	ITO/CdS thin film/N719/P3HT/Ag	Spray Pyrolysis
A5	ITO/CdS thin film/N3/P3HT/Ag	Spray Pyrolysis
B0	ITO/CdS thin film	Chemical Bath Deposition
B1	ITO/CdS thin film/P3HT/Ag	Chemical Bath Deposition
B2	ITO/CdS thin film/Eosin–Y/P3HT/Ag	Chemical Bath Deposition
B3	ITO/CdS thin film/D205/P3HT/Ag	Chemical Bath Deposition
B4	ITO/CdS thin film/N719/P3HT/Ag	Chemical Bath Deposition
B5	ITO/CdS thin film/N3/P3HT/Ag	Chemical Bath Deposition
D0	ITO/CdS powder	CBD + Doctor Blade
D1	ITO/CdS paste/P3HT/Ag	CBD + Doctor Blade
D2	ITO/CdS paste/Eosin–Y/P3HT/Ag	CBD + Doctor Blade
D3	ITO/CdS paste/D205/P3HT/Ag	CBD + Doctor Blade
D4	ITO/CdS paste/N719/P3HT/Ag	CBD + Doctor Blade
D5	ITO/CdS paste/N3/P3HT/Ag	CBD + Doctor Blade
F0	ITO/CdS nanosphere	Hydrothermal
F1	ITO/CdS nanosphere/P3HT/Ag	Hydrothermal
F2	ITO/CdS nanosphere/Eosin–Y/P3HT/Ag	Hydrothermal
F3	ITO/CdS nanosphere/D205/P3HT/Ag	Hydrothermal
F4	ITO/CdS nanosphere/N719/P3HT/Ag	Hydrothermal
F5	ITO/CdS nanosphere/N3/P3HT/Ag	Hydrothermal

3.11. Characterization of Produced Samples

Structural characterization of the produced samples was carried out by X–ray diffraction measurements (Rigaku D/Max–IIIC diffractometer) between 10–70° at RT and with 0.02° steps using CuKα rays. Surface morphology and determination of atomic ingredient of the samples were examined using scanning electron microscopy (SEM, JEOL JSM 6610) and energy dispersed X–ray spectroscopy (EDS, Oxford Instruments), respectively. The optical transmittance and absorption spectra of the samples were measured with a UV–VIS spectrophotometer (SpectraMax M5) instrument in the 400–1000 nm wavelength range. Photoluminescence measurements were made by Dongwoo Optron device with Xe lamp with a power of 450 W at RT in the range of 300–1000 nm. For CdS samples, a 325 nm was used as a stimulation wavelength, while the laser with a 532 nm as an excitation wavelength was employed for the other samples. Current density – Voltage (J–V) measurements of the produced CdS–based HSCs were made with a calibrated solar simulator (AM 1.5D) with an output power of 93 mW/cm^2 via Keithley 2410 source meter. Characterization devices are shown in Figure 3.14 (a)–(d).

Figure 3.14. Photographs of the characterization devices of (a) Rigaku D/Max-IIIC diffractometer (b) JEOL JSM-6610 SEM (https://www.jeol.co.jp/en/products/detail/JSM-6610series.html) (c) SpectraMax M5 and (d) Dongwoo Optron.

4. RESULTS AND DISCUSSIONS

4.1. Structural Properties of Samples

Structural analysis of A0, B0, D0 and F0 samples were examined by X–ray diffraction (XRD) measurements and the results are presented in Figure 4.1 (a)–(d), respectively.

XRD data of A0 sample is shown in Figure 4.1 (a). It was observed that A0 sample had a polycrystalline structure and consisted of reflection planes (100), (002), (101), (102), (110), (103), (200), (112), (201) and (202). This is an indication that CdS thin films have grown in a hexagonal structure with the JCPDS card number 41–1049. The fact that the intensity of the (101) peak was higher than the other peaks indicates that the CdS sample had a preferential orientation along (101). In addition to the peaks of CdS, reflection planes of the ITO structure were also observed in the XRD pattern. These peaks came from ITO. The a and c crystal parameters of the CdS structure were calculated as 0.414 nm and 0.671 nm using the reflection planes (100) and (002), respectively, from Eq. (6a) that is given below:

$$\frac{1}{d^2{}_{hkl}} = \frac{4}{3}\left(\frac{h^2 + hk + k^2}{a^{\,2}}\right) + \frac{l^2}{c^2} \tag{6a}$$

$$\frac{1}{d^2{}_{hkl}} = \frac{h^2 + k^2 + l^2}{a^{\,2}} \tag{6b}$$

where d is interplanar spacing, $h, k\ and\ l$ are miller indices and a, c are the lattice constants. The average crystalline sizes of the CdS thin films were calculated by the plane of (101) using the Scherrer formula given below:

$$D = \frac{0.94\lambda}{\beta \cos\theta} \tag{7}$$

where D is the crystalline size, λ is the wavelength of the X–ray being used, β is the full width at half maximum (FWHM) in radians, and θ is the Bragg diffraction angle. D value for A0 sample was found as 27.3 nm.

The XRD pattern of B0 sample is given in Figure 4.1 (b). In addition to the reflection planes coming from the ITO, it was seen that there were (111), (220) and (311) reflection planes of CdS. This indicates that CdS thin films have grown in cubic zinc blend structure with the JCPDS card number 75–1546. It was determined that the most intense diffraction peak was along the (111) plane. Using the (111) reflection plane, the lattice parameter value (a) of CdS was determined as 0.577 nm from Eq. (6b). The crystalline size D was found as 11.0 nm by the reflection plane (111) with the help of Scherrer formula.

XRD data of D0 sample including CdS powders is presented in Figure 4.1 (c). As seen from the XRD result, CdS powder sample was composed of reflection planes (111), (200), (220) and (311), indicating that the sample has grown in cubic zinc blend as a polycrystalline structure (JCPDS card no: 75–1546). In addition, it appeared that XRD data had a preferential orientation along (111) plane. Lattice parameter, a, of the CdS structure was calculated by the reflection plane (111) as 0.581 nm, using the Eq. (6b). The D crystalline size of the CdS powder sample was found to be 16.3 nm.

The XRD result of the F0 sample, which was grown in two steps, is shown in Figure 4.1 (d). Reflection planes of (100), (002), (101), (110), (103) and (112) of CdS were found in the XRD pattern. This situation was interpreted as CdS nanospheres growing in hexagonal structure with the JCPDS card number 41–1049. It was observed from the XRD pattern that there was a preferential orientation along the reflection plane of (002). In addition to the peaks of the CdS structure, a large number of peaks resulting from ITO were found. With the help of peaks (002) and (110), a and c lattice constants of CdS were calculated from the Eq. (6a) and the results were in turn determined as 0.411 nm and 0.669 nm. The D crystalline size of the CdS nanospheres was calculated as 15.4 nm through the reflection plane (002).

It can be seen from the results discussed above that CdS samples that have different morphologies grown by different methods had different crystal structures, different orientations and different crystalline sizes. It is frequently observed in literature studies that CdS sample (A0), which is generally produced by spray pyrolysis method, has a hexagonal crystal structure that is grown along the reflection planes of (101) (Yılmaz, 2015). On the other hand, the growth of hexagonal CdS samples along the reflection planes of (002) is much more likely because it provides lowest free surface energy. This situation occurs in CdS

nanospheres (F0) obtained in two steps by hydrothermal method. In addition, it can be seen from the literature studies that CdS samples (B0 and D0), which are grown via the chemical bath deposition technique, generally crystallize in the cubic crystal structure (Khallaf, Oladeji, Chai, & Chow, 2008).

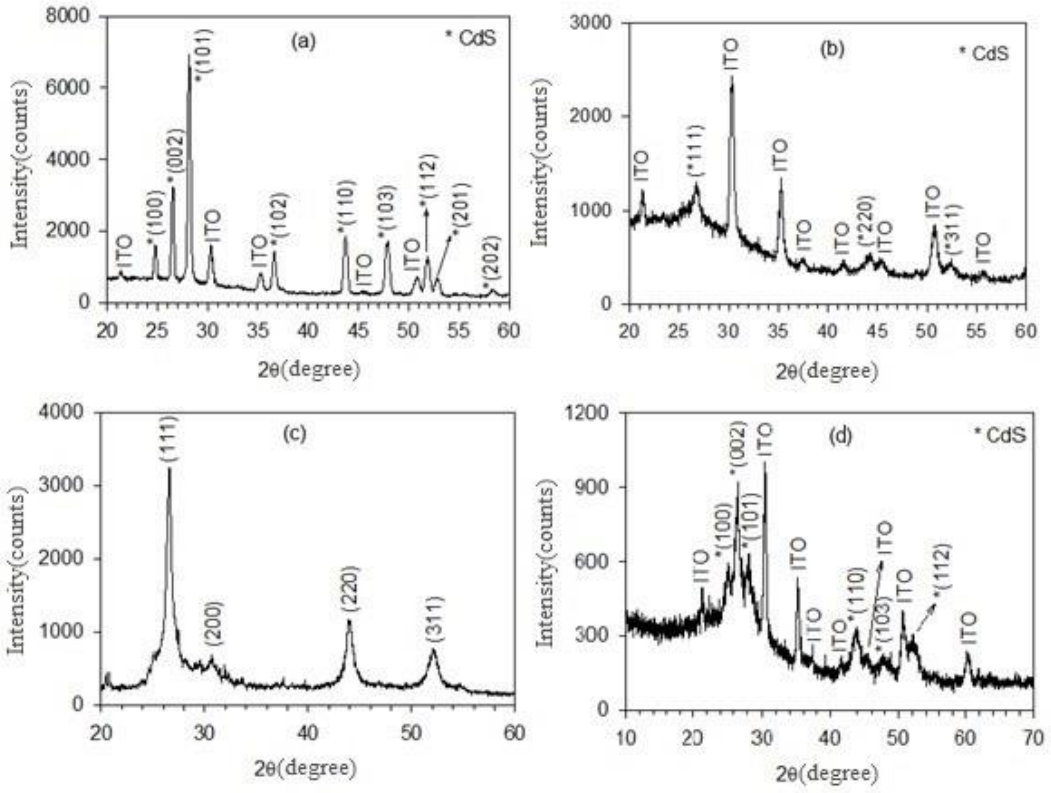

Figure 4.1. XRD patterns of (a) A0, (b) B0, (c) D0 and (d) F0 samples.

4.2. Morphological Analysis of Samples

SEM measurements were performed to obtain the knowledge about the surface morphology and thickness of the produced samples.

Figure 4.2 (a) and (b) indicate surface and cross–sectional photographs of A0 sample. It can be said that CdS thin films consisted of approximately round shaped grains and their grain sizes were distributed nonuniformly on the surface, thus forming small and large sized grains on the sample surface. However, it was seen that the surface had a compact morphology and no voids was observed on the surface. It can be seen that the average thickness value of the film was about 166 nm (Figure 4.2 (b)). Surface and cross–sectional SEM photographs of A1 sample are presented in Figure 4.2 (c) and (d). As seen in Figure 4.2 (c), the P3HT thin film

consisted of very small grain sizes and grains were distributed homogenously on the surface. It was determined that the P3HT layer was properly coated on the CdS thin film and the average thickness of the P3HT thin film was nearly 238 nm (Figure 4.2 (d)).

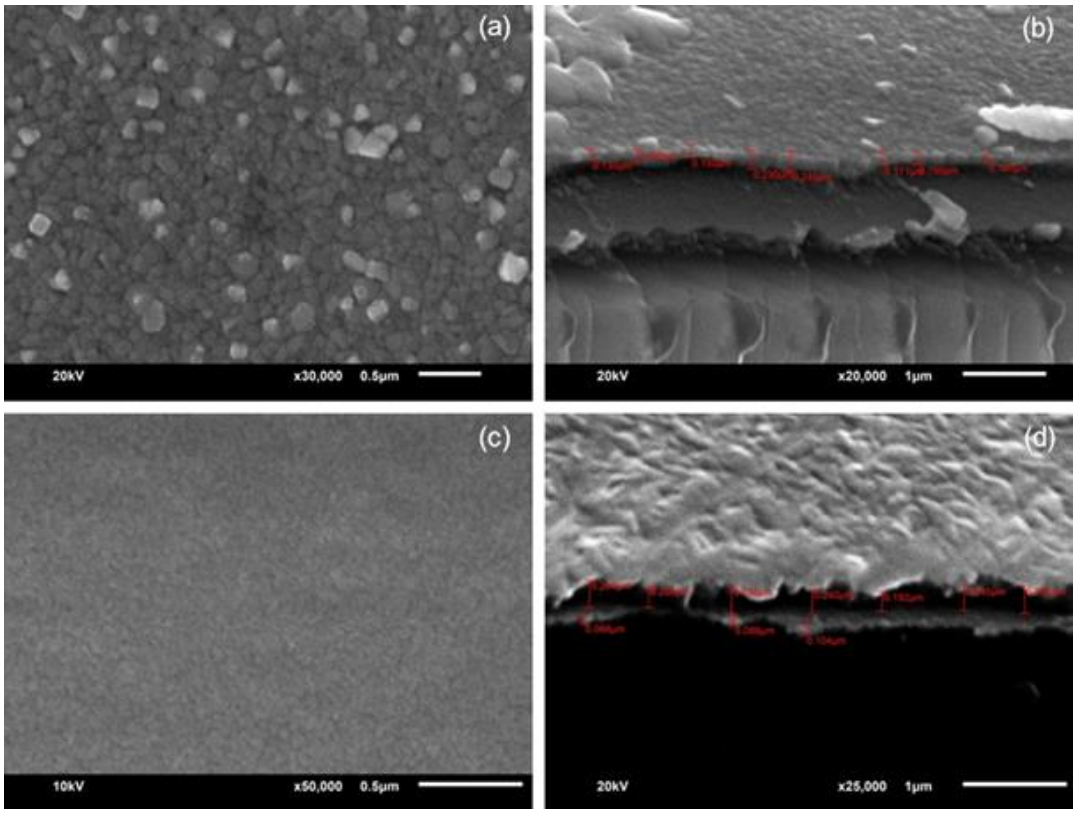

Figure 4.2. (a)–(b) show the plain view and 60° tilted SEM photographs of A0 sample, respectively. (c)–(d) indicate the top view and 60° tilted SEM photographs of A1 sample, respectively.

Figure 4.3 exhibits SEM data of B0 and B1 samples. In Figure 4.3 (a) and (b), surface and cross–sectional images of B0 sample are given. The grain sizes of CdS thin films were too small to be seen due to the formation of very thin layer. A smooth and crack–free CdS surface with a compact morphology was observed. In addition, it was seen that the sample consisted of well–interconnected grains. The average thickness value of the B0 sample was almost 71 nm (Figure 4.3 (b)). SEM photographs of B1 sample are given in Figure 4.3 (c) and (d). It can be seen in the Figure 4.3 (c) that the P3HT thin film consisted of rounded grains and the grain distribution was somehow nonhomogeneous. That is, some grains had a diameter of 500 nm, while others have diameter values below 100 nm. In addition, it was seen that the grains were slightly interconnected and hence, some voids were formed on the surface of the P3HT film. On the other hand, it was determined that the P3HT layer was homogeneously coated on CdS

thin films and the average thickness value was nearly 392 nm (Figure 4.3 (d)).

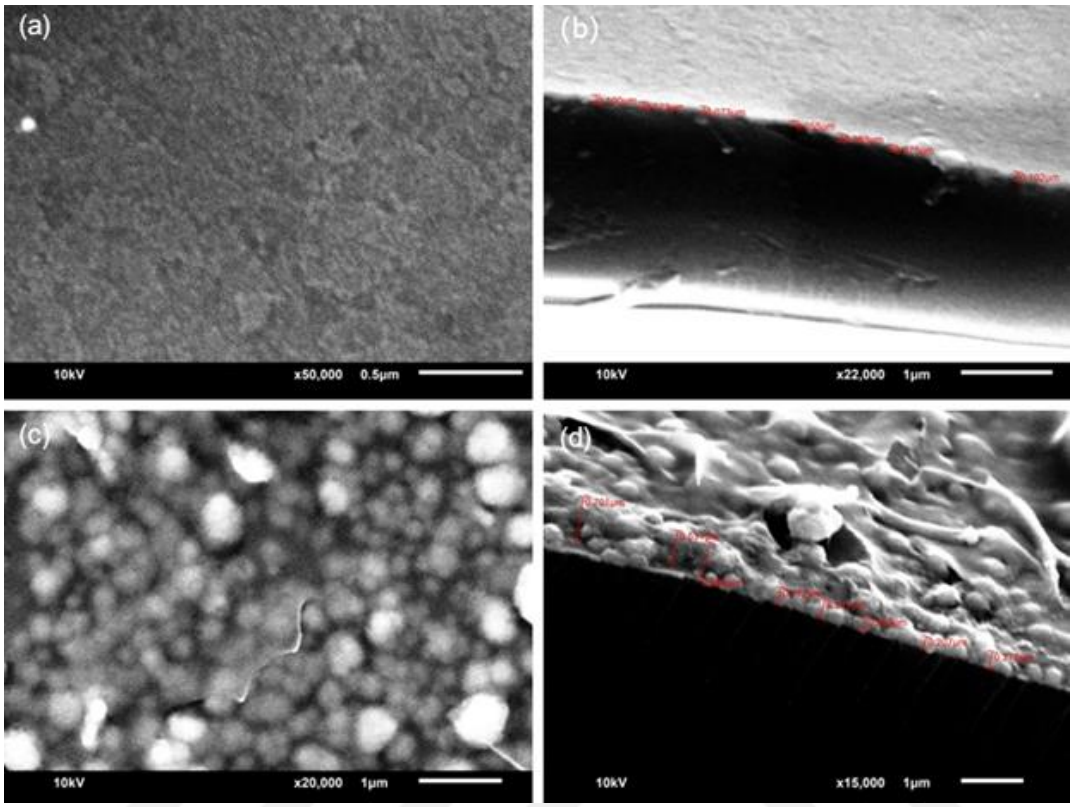

Figure 4.3. (a) the plain view and (b) 60° tilted SEM photographs of B0 sample, (c) the top view and (d) 60° tilted SEM photographs of B1 sample.

Figure 4.4 displays SEM photographs of D0, D1 and D4 samples, respectively. The surface photograph of the D0 sample is given in Figure 4.4 (a). CdS powders appeared to be formed by the combination of nanocrystalline small grains with a hollow and hierarchical morphology. After the P3HT thin film coating was applied on the CdS paste–formed structure, it was observed that the hollow structure of the CdS powders was largely filled by the P3HT layer (Figure 4.4 (b)). However, it was found that the hierarchical structure was preserved. On the other hand, a different surface morphology emerged for D4 sample (Figure 4.4 (c)); a porous and granular morphology appeared for the surface of P3HT. This situation can be commented by that N719 dye modification homogenizing the CdS paste surface makes possible a more uniform P3HT thin film coating. However, the P3HT surface appeared to be rough. The thickness value of the D4 sample was approximately 28 µm (Figure 4.4 (d)). The fact that the thickness is such a high value is due to the thickness of CdS paste fabricated.

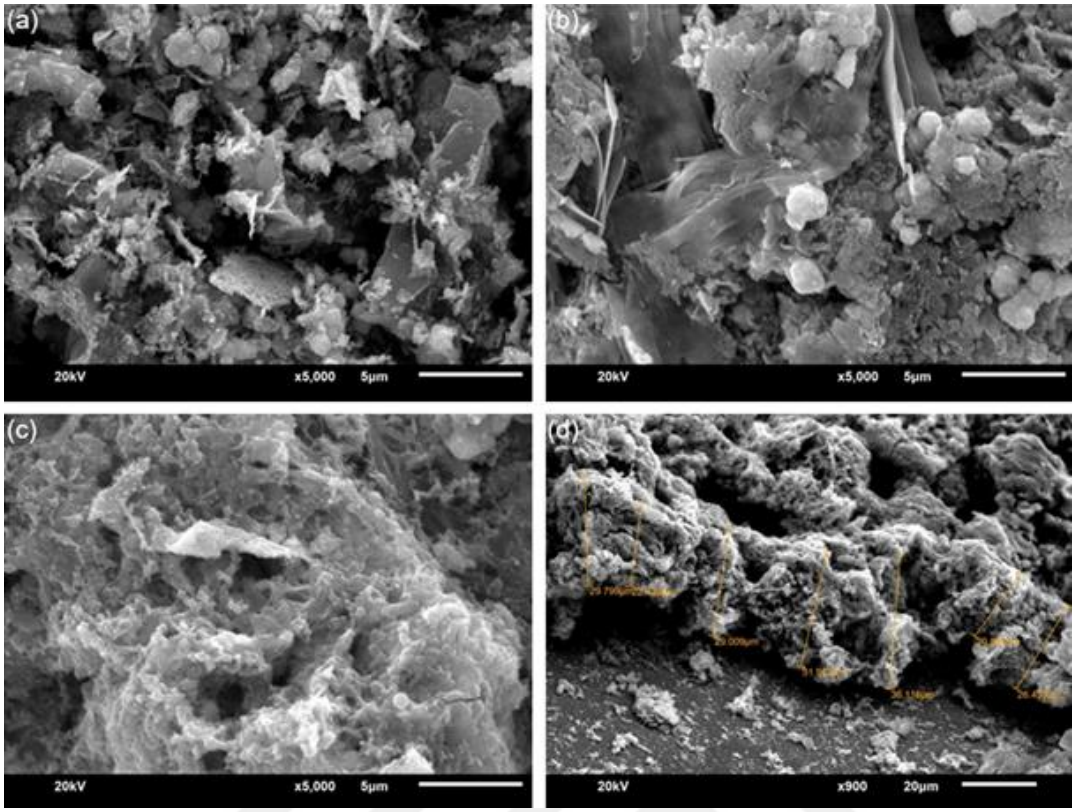

Figure 4.4. Top view SEM photographs of (a) D0 and (b) D1 samples, (c) the top view and (d) 60° tilted SEM photographs of D4 sample.

Figure 4.5 shows SEM photographs of F0, F1, F2 and F4 samples. As seen in Figure 4.5 (a), the F0 sample grew in the nano–dimensional spherical morphology. It was observed that each sphere was formed by the combination of small sized CdS nanocrystals. It was determined that the diameter distributions of CdS nanospheres were somewhat homogeneous. A compact and dense sphere surface morphology was obtained. No cracks and/or voids were observed on the sample surface. In addition, large CdS nanospheres were found to grow on smaller diametered CdS spheres. It was determined from Figure 4.5 (b) that the average thickness value of CdS nanospheres was around 289 nm. SEM data of F1 sample is given in Figure 4.5 (c). It was observed that the P3HT layer growing on the CdS layer consisted of spherical grains. It was determined that some spheres with large sizes were formed on small spheres. It was seen that the P3HT coating on the samples modified with Eosin–Y and N719 dyes was marginally different from that of unmodified ones. Sphere sizes of F2 and F4 samples were observed to be almost homogeneous. It was determined that a compact, crackless and dense CdS nanosphere morphology occurred. The average thickness of the F4 sample was found to be nearly 397 nm. Therefore, the thickness of P3HT layer was observed to be about 108 nm.

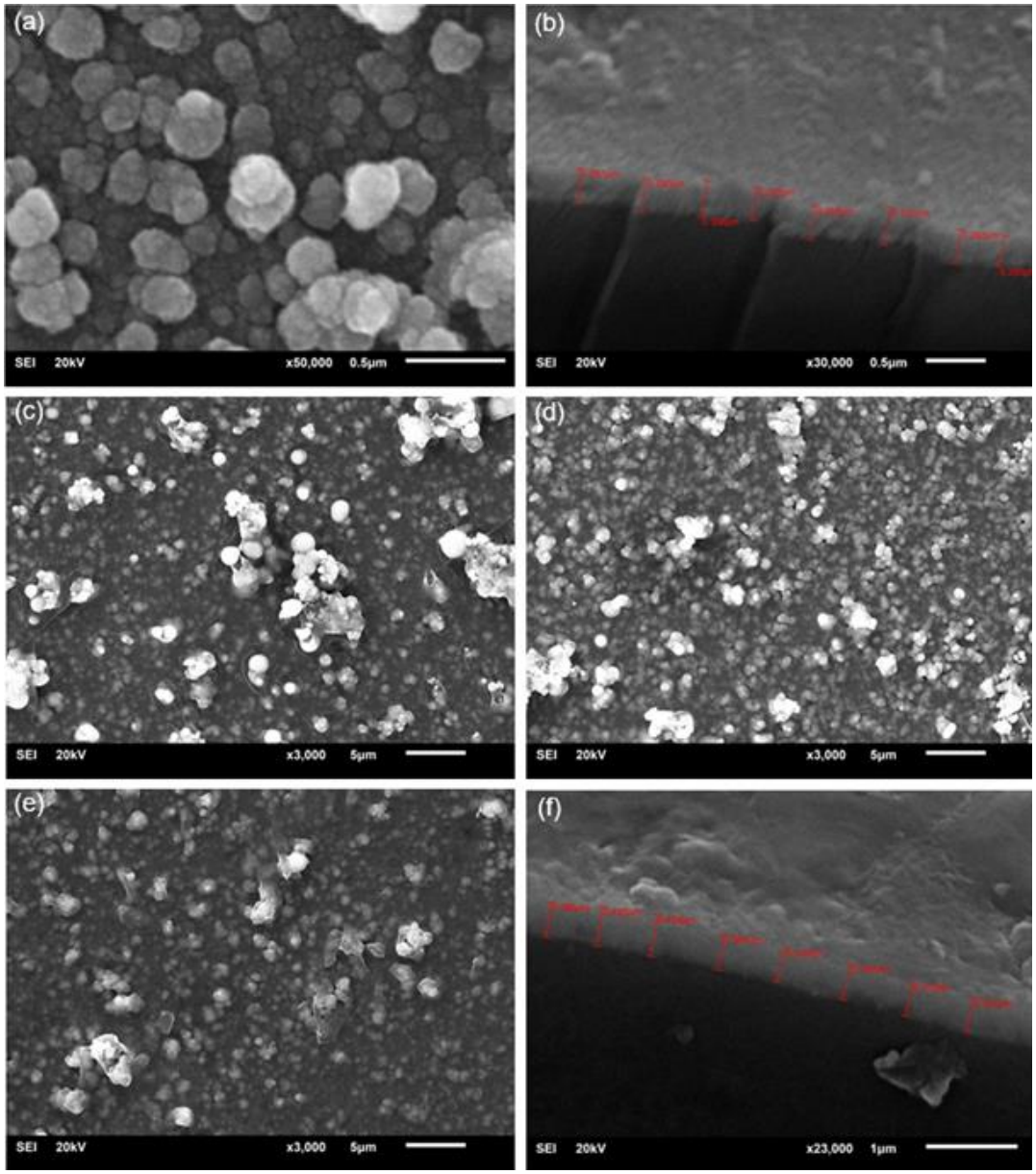

Figure 4.5. (a) top view and (b) 60° tilted SEM photographs of F0 sample, plain view SEM photographs of (c) F1, (d) F2 and (e) F4, respectively and (f) the 60° tilted SEM photographs of (e).

4.3. Elemental Composition Analysis (EDS) of Samples

The chemical composition of the produced CdS samples was investigated by EDS analysis. Figure 4.6 (a) illustrates the EDS spectrum of the A0 sample. The spectrum shows the peaks of the Cd and S elements. The fact that the percentage concentration of the Cd atom is slightly different from that of the S atom indicates almost stoichiometric thin film formation. On the other hand, the EDS spectrum of B0 sample is given in Figure 4.6 (b). From the data obtained for CdS thin film, it was determined that the percentage atomic concentration of Cd was 54.5

while it was 45.5 for S. This showed that the CdS main structure was richer in terms of Cd atom. EDS analysis of D0 and F0 samples are presented in Figure 4.6 (c) and (d), respectively. As can be seen, while D0 sample was richer in Cd atom, there was an excess of S atom in F0 sample. Such deviations from stoichiometry cause CdS samples to grow nonstoichiometrically and trigger the formation of internal defects such as Cd vacancies (V_{Cd}), Cd interstitials (I_{Cd}), S vacancies (V_S) and S interstitial (I_S) (Yılmaz et al., 2019).

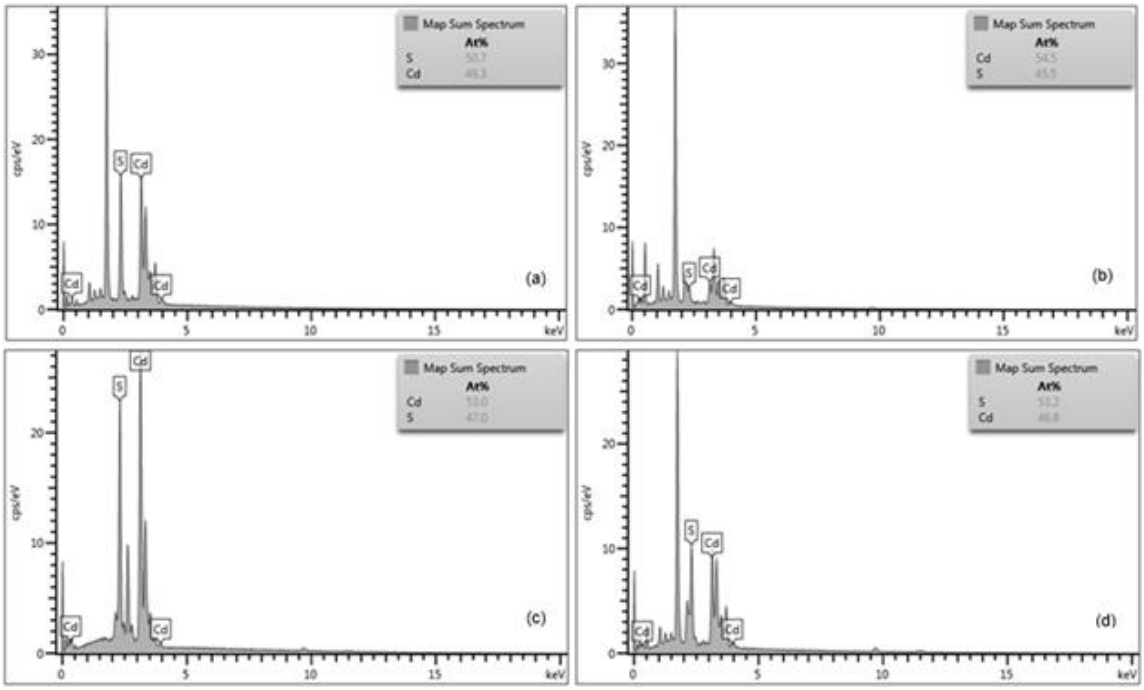

Figure 4.6. EDS spectra of (a) A0, (b) B0, (c) D0 and (d) F0 samples.

4.4. Investigation of Optical Properties of Samples

Optical properties of the samples were examined by transmittance, absorption and RTPL measurements.

Figure 4.7 (a)-(e) depict the transmittance curves of A0, B0, D0, F0 and P3HT sample grown on ITO, respectively. From the Figure 4.7 (a), it was seen that the transmittance value of CdS thin films was approximately 80% in the range from 520 nm to 1000 nm, indicated that the transmittance value of the produced samples was very good and can be used as a window layer in SCs. In addition, the sharp increase at the absorption edge demonstrated that the quality of CdS sample was good. The transmittance curve of the B0 sample is given in Figure 4.7 (b). It was seen that an increase has occurred in the absorption edge starting from 500 nm. However, the fact that this increase was edgeless indicated that the crystal quality of the

produced sample was not very good. The transmittance curve showed an increasing behavior with increasing wavelength and the maximum transmittance value occurred at a wavelength of 1000 nm as 60%. On the other hand, the transmittance curve of the D0 powder sample is presented in Figure 4.7 (c). It was seen that the transmittance value of CdS powder sample was in the range of 1–1.5%. This is thought to be due to the thickness factor formed in the measurement of the transmittance value of the powder sample. As the wavelength reached 650 nm, the transmittance value increased gradually. Figure 4.7 (d) shows the transmittance curve of the F0 sample. It was observed that the transmittance value was at the highest as 20% up to approximately 520 nm. After 520 nm, the transmittance increased subsequently and it was 45% at 1000 nm wavelength value. The transmittance curve of organic P3HT material grown by spin–coating on ITO is illustrated in Figure 4.7 (e). Although the P3HT material coated on ITO or CdS appeared in dark color, its transmittance appears to be as high as approximately 90% in the 650–1000 nm wavelength range.

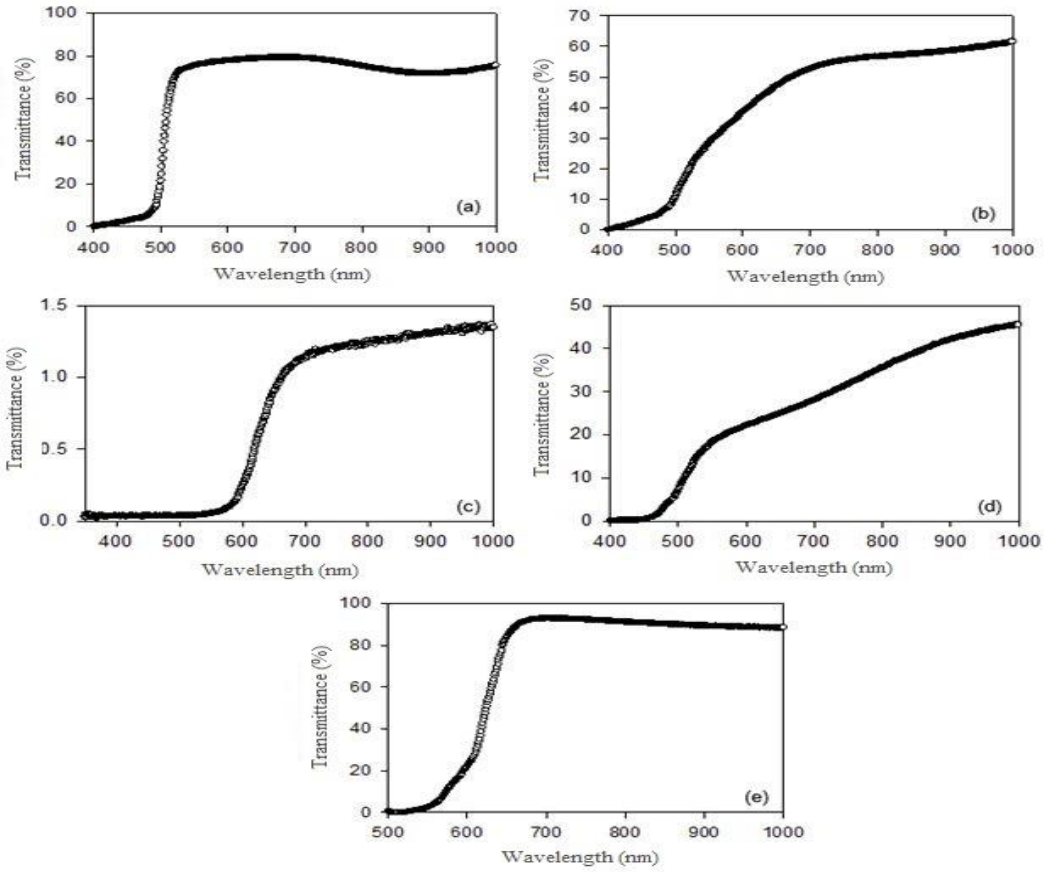

Figure 4.7. Transmittance spectra of (a) A0, (b) B0, (c) D0 and (d) F0 samples, (e) transmittance curve of P3HT film grown on ITO substrate.

The band gap values of the samples were calculated with Tauc's plot analysis method and the results are shown in Figure 4.8 (a)–(e). Figure 4.8 displays the band gap values of A0, B0, D0, F0 and the P3HT sample grown on ITO, respectively. It can be seen from Figure 4.8 (a)-(b) that the band gap values of the A0 and B0 samples were obtained as 2.45 eV and 2.98 eV, respectively. On the other hand, the band gap value of D0 sample was found as 1.92 eV. The band gap value of the F0 sample was revealed to be 2.52 eV. The difference between the band gaps values of CdS samples produced by four different methods can be interpreted as follows: as known, the RT band gap value of the bulk CdS material is 2.42 eV. The higher band gap value of the A0 sample than that of bulk one can be attributed to the slight deviations from stoichiometry of CdS thin films and to the formation of some defects in the crystal structure. The high bandwidth values of B0 and F0 samples may correspond to a situation expressed as quantum confinement effect (Chuu & Dai, 1992). As known, this effect occurs when the crystalline size of the CdS sample drops below a certain value and this leads to significant increases in band gap value. It can be said from XRD and SEM results that such a situation has occurred. Increasing bandwidth value causes CdS samples to be used as a window layer more efficiently in SCs. However, it is thought that the band gap value of the D0 sample is below that of bulk one due to the thickness factor. It is known that increasing film thicknesses leads to a drop in band gap values (Lamouri, Salmani, Ez-zahraouy, & Benyoussef, 2016). On the other hand, the band gap value of the P3HT thin film was calculated as 1.98 eV and is shown in Figure 4.8 (e). This value is in agreement with the value recorded in the literature studies (Kroon, Lenes, Hummelen, Blom, & de Boer, 2008; Dou, Liu, Hong, Li, & Yang, 2015).

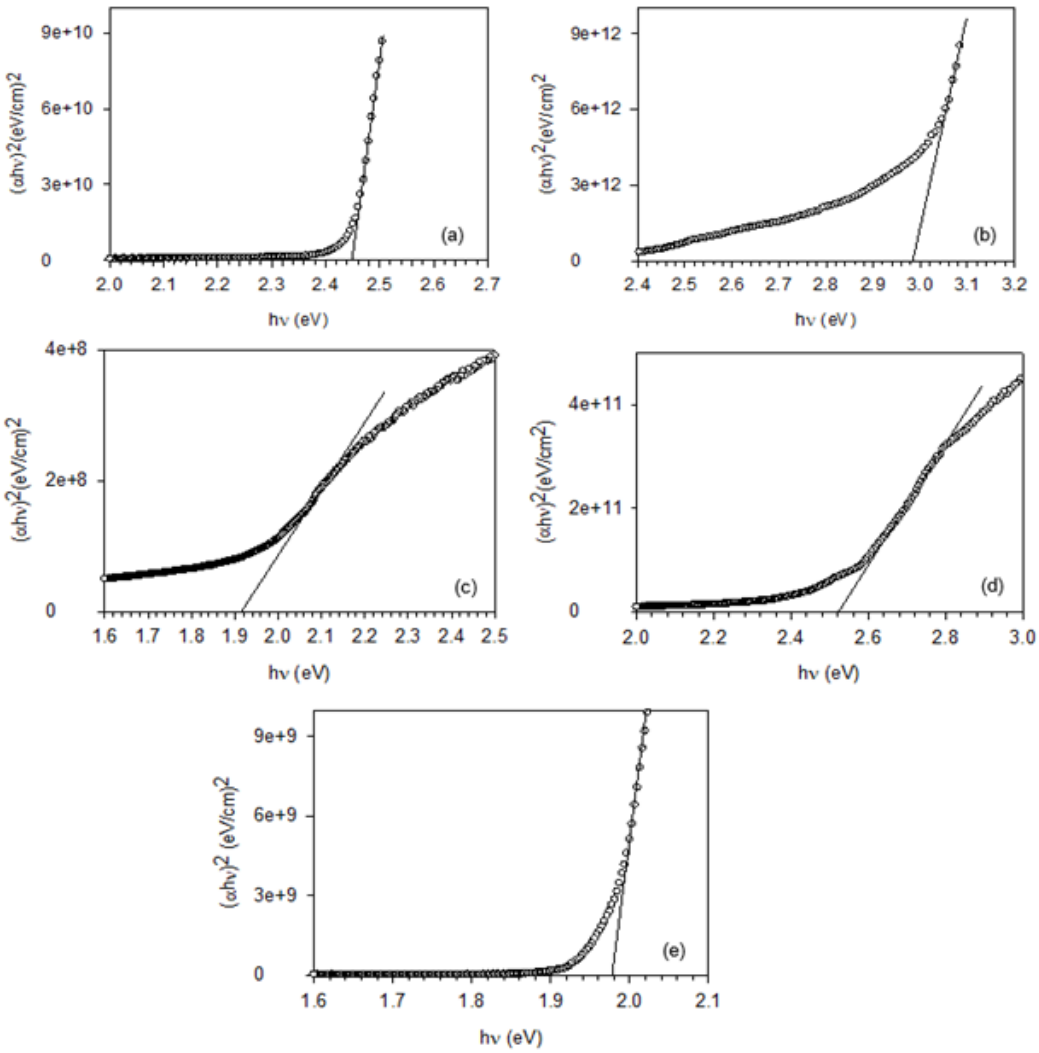

Figure 4.8. Tauc's plot analysis results of (a) A0, (b) B0, (c) D0 and (d) F0 samples, (e) band gap curve of P3HT film grown on ITO substrate.

Absorption spectra of samples containing different dyes (Eosin–Y, D205, N719 and N3) were taken to investigate the effects of dye modification on the CdS surface. Figure 4.9 (a)–(d) show the absorption spectra of the sample series of A, B, D and F, respectively. While A1, B1 and F1 samples exhibited absorption band in the range of 400–650 nm, this interval value was wider for D1 sample. In addition, with the dye modification, some shifts towards longer or shorter wavelengths in A, B, D and F series samples occurred. This situation is related to the increase or decrease of photon capture ability of the formed CdS sample. A1, B1 and F1 samples had maximum peak values at 483 nm, 483 nm and 468 nm, respectively. These peaks are associated with vibrational transitions that exist between polymer chains of the P3HT molecule resulting from strong interchain interactions (Kim, An, Oh, Chung, & Park, 2014). In the D1 example, this peak was nonobvious at all. Within A, B and F series samples, the

absorption intensity increased for all of the dye modified samples compared to the non–modified (A1, B1 and F1) ones. However, the D series examples displayed a slightly different behavior. Only the Eosin–Y dye modified sample (D2) had an increase in absorption. The increase in peak intensities of absorption spectra after dye modifications is an indication that these dyes were absorbed efficiently on the CdS surface. Such a situation leads to the emergence of a more compatible CdS/P3HT interface. This improvement is due to the strong π–π interactions between the P3HT polymer chain and any dye used (Nan et al., 2013).

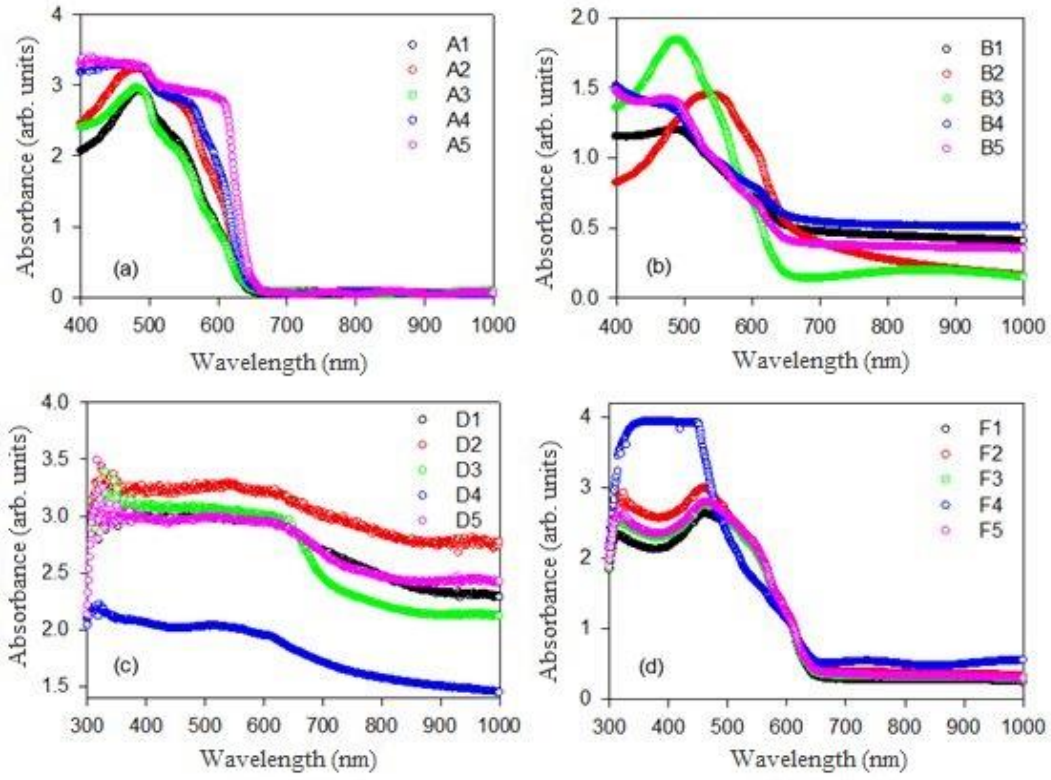

Figure 4.9. Absorption spectra of (a) A series, (b) B series, (c) D series and (d) F series samples.

The defect structure of CdS and P3HT samples were examined by RTPL measurements and the results are shown in Figure 4.10 (a)–(e). Figure 4.10 (a)–(d) depict the PL spectra of samples A0, B0, D0 and F0, respectively. A0 sample showed two basic peaks corresponding to 503 nm and 680 nm wavelengths. The first peak belongs to the green zone and is associated with the band gap value of the CdS material resulting from radiated recombination of excitons (Yow-Jon Lin, You, Chang, Liu, & Wu, 2015), while the second peak had an asymmetrical nature between 525 nm and 800 nm and is called as deep level emission. This peak is often attributed to point defects such as sulphur vacancies (V_S), cadmium vacancies (V_{Cd}) and

cadmium interstitials (I_{Cd}) (Yılmaz et al., 2017). PL data of B0 sample is given in Figure 4.10 (b). CdS thin films grown through the CBD appeared to have a wide asymmetrical peak with a maximum wavelength of 619 nm. This peak covers all regions starting from the blue zone to the red zone. The origin of this peak can be attributed to above–mentioned (I_S, I_{Cd} and V_S) defects. In addition to the mentioned peak, another peak corresponding to the red region of 679 nm wavelength was observed and this peak is attributed to V_{Cd} defects caused by the presence of surface conditions (Yılmaz et al., 2017). The PL curve for D0 sample is presented in Figure 4.10 (c). The CdS powder sample appeared to exhibit peaks essentially corresponding to three different regions. These zones are 350–400 nm (UV), 400–500 nm (blue) and 500–750 nm (deep level emission), respectively. The fact that CdS powders grew nonstoichiometrically causes such intrinsic defects. While the UV peak is associated with transitions between shallow and deep levels, the blue peak is attributed to defect levels (Yılmaz, Atasoy, Tomakin, & Bacaksız, 2015). On the other hand, deep level emission is generally attributed to intrinsic defects such as I_{Cd}, V_S and V_{Cd}, as mentioned above (Yılmaz et al., 2017). The PL spectrum of CdS nanospheres (F0) is shown in Figure 4.10 (d). As in the D0 example, CdS nanospheres were also shown to have peaks with 350–400 nm (UV), 400–500 nm (blue) and 500–750 nm (deep level emission) wavelength ranges. The origin of these peaks was discussed in detail above. It was determined from the Tauc band gap calculation that the band gap value of CdS nanospheres was 2.52 eV (492 nm). This wavelength corresponds to the blue region. Yet, the bulk value of the CdS material corresponds to the green zone with 2.42 eV. However, the fact that the CdS sample has grown in nanoscale led to an increase in the band gap value, thereby creating a shift towards the blue region in the PL curve. As a result, it can be said that the blue peak also corresponds to the bandwidth of the CdS nanospheres (Thambidurai et al., 2010). The PL curve of the P3HT thin film grown on ITO is given in Figure 4.10 (e). As can be seen, the P3HT film basically displayed an asymmetrical peak.

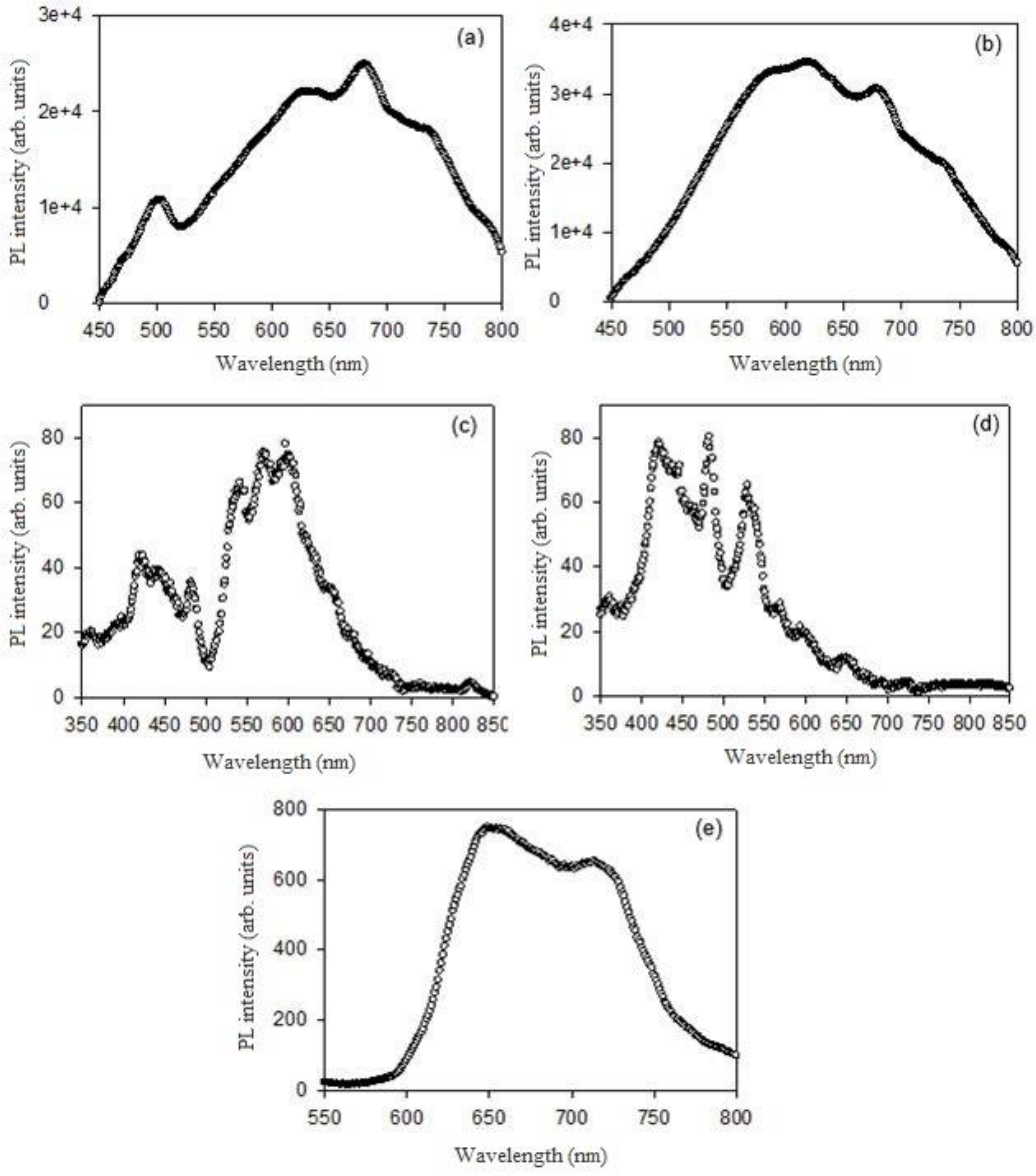

Figure 4.10. Photoluminescence curves of (a) A0, (b) B0, (c) D0 and (d) F0 samples, (e) photoluminescence spectrum of P3HT film grown on ITO substrates.

RTPL curves of A, B, D and F series heterostructures are shown in Figure 4.11 (a)–(d), respectively. Figure 4.11 (a) shows the PL curves corresponding to A1, A2, A3, A4 and A5 samples, respectively. Compared to that of Figure 4.10 (e), it can be said that similar PL curves occurred. This means that the P3HT thin film dominated all spectra of PL data. The only variable thing was peak intensities. Compared with A1 heterostructure, a decrease in the peak intensity of the other A series heterostructures took places. A similar behavior was recorded in B and D series examples (Figure 4.11 (b)–(c)). Such a situation is an indication of the effective electron transfer from the P3HT layer to the CdS layer with different dye

modifications of the CdS surfaces. This results in efficient exciton separation at the CdS/P3HT interface (M. Zhong et al., 2012; Jiang et al., 2010). Thus, dye modification causes more suitable interface formation between CdS and P3HT. This is in agreement with the optical absorption results discussed earlier. Similar results were obtained by Jabeen, Adhikari, Pathak, Shah and Nunzi (2018) for CdS–based HSCs. On the other hand, as for F series samples, the PL intensity of the F1 sample was greater than the intensities of all the other peaks, except for F3 sample. The peak intensity of the F3 sample was more intense than that of F1 sample, meaning that there will be no effective exciton dissociation at the CdS/P3HT interface, which significantly reduces the efficiency of the SC.

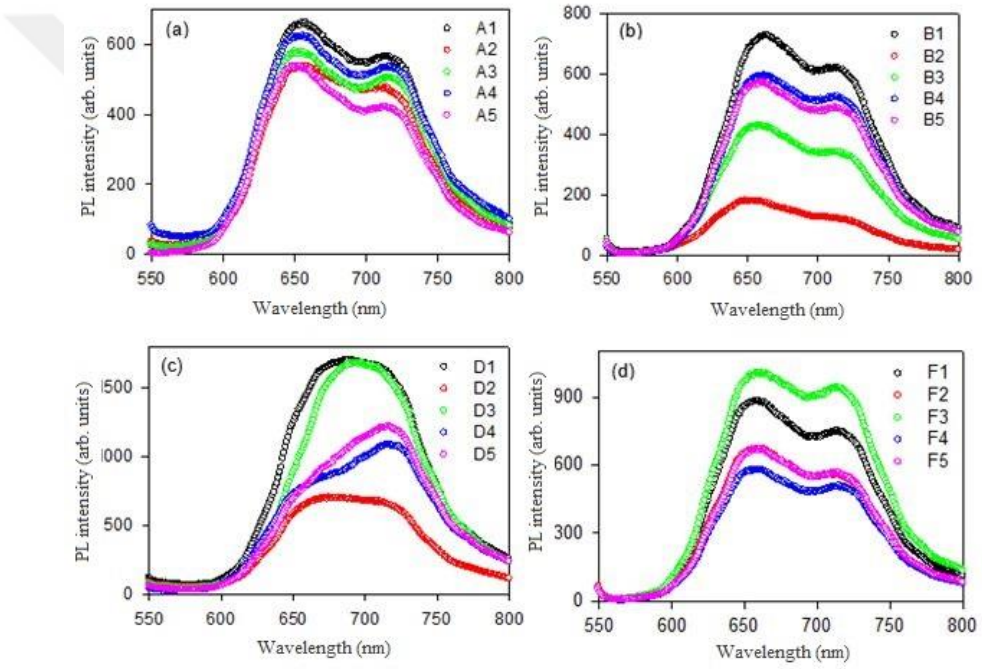

Figure 4.11. Photoluminescence curves of (a) A series, (b) B series, (c) D series and (d) F series heterostructures.

Current density – voltage (J–V) measurements of heterostructures belonging to A, B, D and F series were measured under the calibrated light and the results are shown in Figure 4.12 (a)–(d). Figure 4.12 (a) shows the J–V curves of A1, A2, A3, A4 and A5 samples, respectively. In addition, important parameters of the produced SCs such as short circuit current density (J_{sc}), open circuit voltage (V_{oc}), filling factor (FF) and solar cell efficiency Ƞ (%) are listed in Table 4.1. All SCs clearly showed a photovoltaic effect. J_{sc} value of A1 sample was 0.30 mA/cm^2, V_{oc} value was 0.14 V, filling factor was 0.33 and PCE was 0.015%. The low value of this

efficiency is due to the weak contact area of the hydrophilic CdS and P3HT surfaces (M. Zhong et al., 2012). In addition, as seen in the PL results in Figure 4.10 (a), it is thought that CdS thin films that had a defected structure may lead to low SC efficiency (Chen et al., 2011). Compared with the A1 sample, an increase in the V_{oc} value of the A2 sample, whose CdS surface has been modified with Eosin–Y dye, from 0.14 V to 0.49 V was observed. This corresponds to a fourfold increase in PCE value of approximately 0.057%. The reason for such an increase in the V_{oc} value is that surface modification with Eosin–Y dye causes direct contact between the CdS and P3HT layers, thereby reducing charge recombination between the electrons in the CdS layer and the holes in the P3HT layer (Lim et al., 2013; Thitima, Patcharee, Takashi, & Susumu, 2009). Efficiency value of A3 sample containing D205 dye was obtained as 0.059%. This value is higher than that of the efficiency of the sample without any dye treat (A1). This can be attributed to an improvement in the wettability of the CdS thin film surface because the interaction between water and dye molecules results in the formation of a hydrophobic surface (Ruankham et al., 2013). In addition, a dipole moment of the D205 molecule causes a shift in the locations of band energy between CdS and P3HT, which leads to an increase in the open circuit voltage of the SC (Ruankham et al., 2013). On the other hand, the best efficiency value was obtained as 0.082% for A4 sample. As can be seen from Table 4.1, N719 dye modification improves not only the J_{sc} value of the cell but also the V_{oc} value. Compared with the other A series cells, there was no significant change in J_{sc} value, while the maximum V_{oc} (0.69 V) value is displayed by A5 sample. The efficiency value of this SC was 0.080%. Such improvements in the efficiency of SCs containing Ru–based dyes can be explained by the enhancement of the electronic coupling between the CdS and N719 or N3 dye adhering to the CdS surface (Nan et al., 2013). Comparable results were found by Yun-Yue Lin et al. (2009) for TiO_2/P3HT HSCs and by M. Zhong et al. (2012) for CdS/P3HT HSCs.

J–V curves of B1, B2, B3, B4 and B5 samples are given in Figure 4.12 (b). While the efficiency value of the sample without dye modification (B1) was 0.046%, no significant efficiency change was observed as a result of modification of CdS surface with Eosin–Y. With the D205 dye modification, the efficiency value of the cell increased. Efficiency was reached to 0.153% with the N719 dye modification. However, the highest PCE was obtained for B5 sample as 0.322%. The reasons for such improvements in open circuit voltage and short circuit currents are mentioned in detail above. In addition, there was an improvement in

photon absorption efficiency as previously discussed in the absorption spectra (Figure 4.9) with the surface modification of the CdS thin film with different dyes. This is due to the formation of a better surface contact area between CdS and P3HT. Furthermore, surface modification with different dyes causes an increase in exciton separation efficiency at the CdS/P3HT interface. As discussed in the PL results (Figure 4.11), there is a dye–induced improvement in the interface compatibility between CdS and P3HT.

CdS thin films (A and B series) obtained by two different methods appeared to have very different efficiency values. As discussed above, the dye adhesion capacities of CdS samples (A0, B0) obtained in different grain sizes are different. Different dyes come into better surface contact in B series heterostructures due to the smaller grain and crystalline sizes that B0 sample has. As a result, higher efficient SCs are attained.

The J–V graphs of the D and F series heterostructures are presented in Figure 4.12 (c)–(d), respectively. For D1 sample without any dye modification, the efficiency value was obtained as 0.046%. For CdS surface modified with the other D205, N719 and N3 dyes, SC efficiency values are even worse than that of D1 sample as seen in Table 4.1. This is in agreement with the absorption plots presented in Figure 4.9 (c). That is, dye modification of CdS paste surfaces with D205, N719 and N3 dyes led to a reduction in absorption curves, thus, CdS paste surfaces were less coated with such dyes. On the other hand, the highest efficiency value in D series was observed for D2 sample as 0.153%. The absorption curve results also support this situation. In addition to the comments on the efficiency improvement caused by Eosin–Y dye modification in the A series heterostructures, Eosin–Y dye helps to reduce leakage currents by direct contact between CdS and Ag metal (Lim et al., 2013).

Figure 4.12 (d) represents the J–V characteristics of the F1, F2, F3, F4 and F5 samples, respectively. The efficiency value of F1 sample was obtained as 0.013%. When the surface of CdS nanospheres was modified with Eosin–Y dye, an improvement in the efficiency value occured. However, as a result of D205 dye modification, there was a significant decrease in SC efficiency. On the other hand, just as the short circuit current density (J_{sc}) of the SC modified by N719 dye reached its maximum value, the open circuit voltage also increased significantly from 0.59 V to 0.92 V. The efficiency value of this SC reached the highest value of 0.881%. On the other hand, while the F5 sample displayed the highest open circuit voltage

(V_{oc}) value, its PCE value was 0.29%. It can be seen from Figure 4.9 (d) that the increase or decrease in the efficiency values are related to the dye absorption property of the CdS nanosphere surface. In addition, such improvements in efficiency value can be explained by the increase in exciton dissociation efficiency at the CdS/P3HT interface. This case is also approved by a decrease in the PL curve of F2, F4 and F5 samples compared to the data of the unmodified sample (Figure 4.11 (d)). However, there was an increase in the PL peak intensity of the F3 sample containing D205 dye, which led to a decrease in efficiency.

Compared with the other series, it is thought that the high efficiency seen in the F series samples is due to the growth of CdS samples in nanosphere morphology. Because CdS samples grown in sphere morphology have more dye absorption due to excessive surface contact area. Such a situation leads to an increase in the PCE of SCs modified by dye.

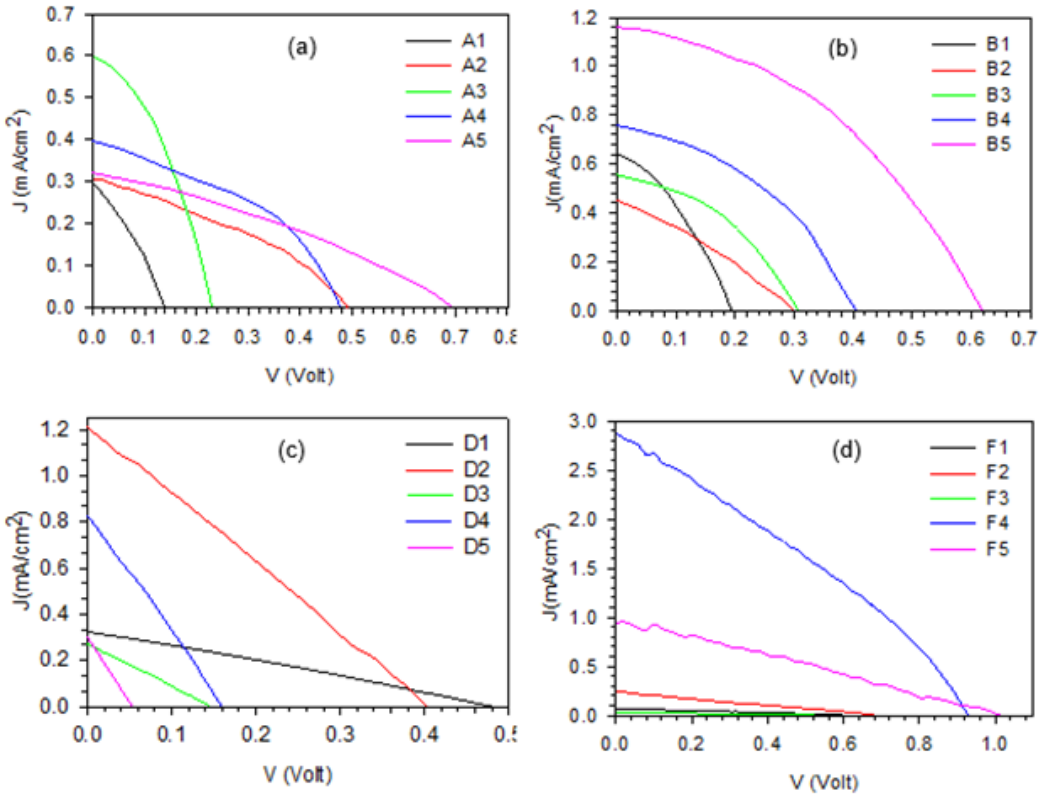

Figure 4.12. J–V characteristics of (a) A series, (b) B series, (c) D series and (d) F series hybrid solar cells.

Table 4.1. Solar cell parameters of A, B, D and F series photovoltaics

Cell Code	J_{sc} (mA.cm^{-2})	V_{oc} (V)	*FF*	*η (%)*
A1	0.30	0.14	0.33	0.015
A2	0.31	0.49	0.35	0.057
A3	0.60	0.23	0.40	0.059
A4	**0.40**	**0.48**	**0.33**	**0.082**
A5	0.32	0.69	0.34	0.080
B1	0.64	0.19	0.35	0.046
B2	0.46	0.30	0.30	0.045
B3	0.56	0.31	0.41	0.080
B4	0.76	0.40	0.41	0.135
B5	**1.16**	**0.62**	**0.42**	**0.322**
D1	0.32	0.48	0.280	0.046
D2	**1.21**	**0.40**	**0.260**	**0.135**
D3	0.27	0.14	0.265	0.011
D4	0.83	0.16	0.264	0.038
D5	0.30	0.05	0.267	0.004
F1	0.068	0.59	0.299	0.013
F2	0.241	0.68	0.256	0.045
F3	0.032	0.52	0.240	0.004
F4	**2.878**	**0.92**	**0.309**	**0.881**
F5	0.956	1.01	0.279	0.290

5. CONCLUSIONS

Within the scope of this thesis, CdS samples with different morphologies were produced by three different methods. CdS–based hybrid solar cells were obtained by these samples in different morphologies. In addition, CdS hybrid solar cells were produced with the obtained heterostructures making surface modifications with different dyes on CdS samples grown in different morphologies. Thus, the structural, morphological, optical and electrical measurements of the samples were examined. The reasons for changes in CdS–based hybrid solar cell efficiency values were discussed in detail.

The obtained results in this thesis are summarized as follows:

i. A0 and F0 samples had a hexagonal crystal structure, however, B0 and D0 samples grew in a cubic zinc blend structure.

ii. It was observed that A0 sample consisted of round shaped and non–homogeneous grains, whereas B0 samples appeared to be in very small grains. It was determined that D0 sample consisted of small–sized nanocrystals with a hierarchical morphology, whereas F0 sample was obtained in nano dimensional sphere morphology. It was noticed that the coating of P3HT thin film covered on CdS samples was homogeneous for all the samples.

iii. From the EDS results, it can be said that the A0 sample had the most stoichiometric in nature. Other samples (B0, D0 and F0) exhibited deviations from stoichiometry.

iv. It was noticed that the transmittance value of the A0 sample was nearly 80% in the range of 520–1000 nm, and the maximum transmittance value of the B0 sample appeared to be 60% at the wavelength of 1000 nm. On the other hand, whereas D0 sample showed very low transmittance as 1–1.5%, F0 sample was found to reach its highest transmittance value at 1000 nm wavelength as 45%. The transmittance of the P3HT film was found to be around 90%.

v. Band gap values of A0, B0, D0, F0 and P3HT samples were found as 2.45 eV, 2.98 eV, 1.92 eV, 2.52 eV and 1.98 eV, respectively.

vi. Increases in absorption peak intensities occurred with any dye modification in A, B and F series samples. However, in D series samples, only the peak intensity of D2 sample increased.

vii. According to the photoluminescence results obtained with a 325 nm excitation wavelength, each of the CdS samples with different morphologies grown by different methods exhibited defect peaks corresponding to different regions.

viii. A decrease in peak intensities in the A, B and D series was observed from the photoluminescence results of CdS–based heterostructures measured by a laser with a wavelength of 532 nm compared to the sample without dye modification. However, in the F series, the F3 sample was found to exhibit an increasing peak intensity.

ix. According to the current density–voltage results, the dye modification of the CdS surface within each series led to an increase in PCE. For example, in the A series, A4 sample had the highest efficiency value, while in B series, the B5 sample had the highest. However, in the D series, the maximum efficiency value was observed for the D2 sample, while in the F series, the F4 sample had the highest solar cell efficiency. In addition, efficiency values of CdS–based solar cells obtained with different morphologies showed different characteristics. It was determined that the F series samples obtained in nanosphere morphology had the maximum solar cell efficiency.

6. RECOMMENDATIONS

As a future study of this thesis, an increase in solar cell efficiency values can be further obtained by creating a PEDOT:PSS layer on ITO substrates. Also, possible changes in solar cell efficiency can be examined by using Au and Al as front contacts. Furthermore, the effect of different dyes and morphologies can be applied to ZnO/P3HT and ZnS/P3HT hybrid solar cells.

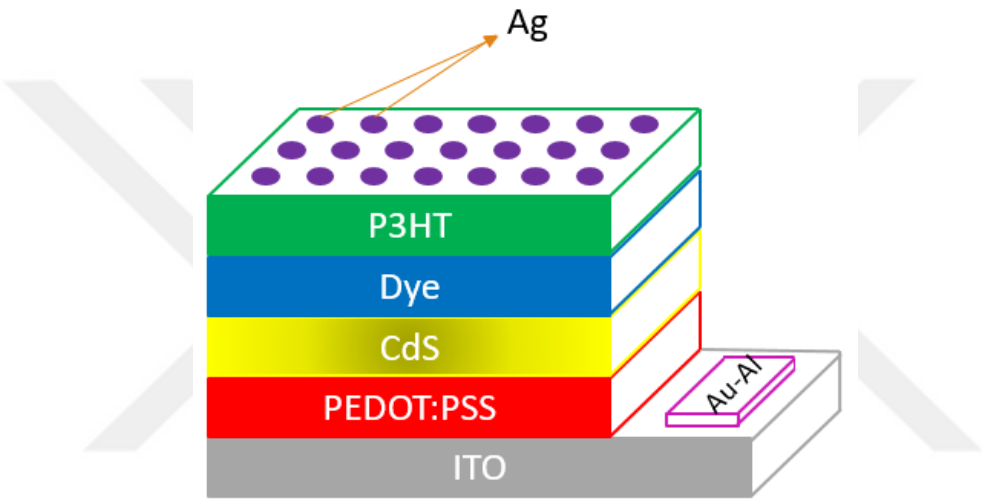

Figure 6.1. Schematic diagram of the PEDOT:PSS/CdS/P3HT hybrid solar cells for the future studies.

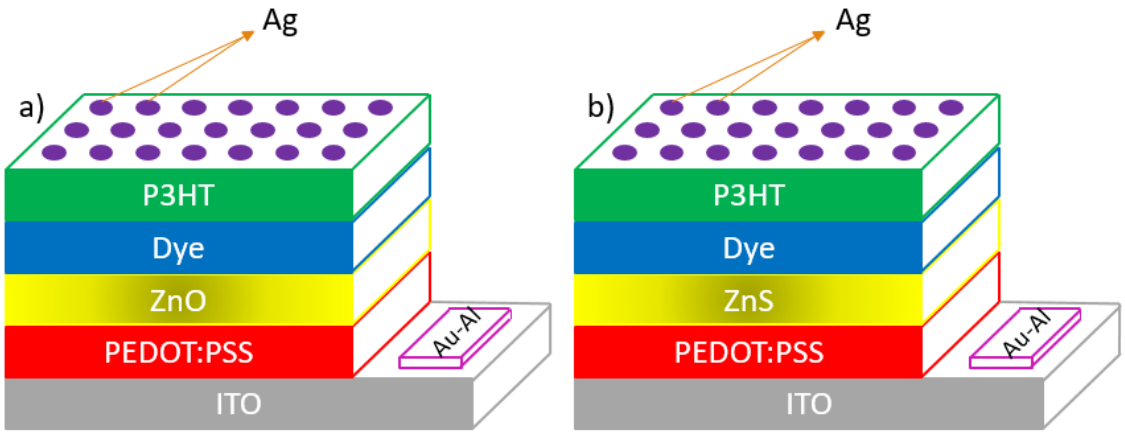

Figure 6.2. Schematic drawing of (a) PEDOT:PSS/ZnO/P3HT and (b) PEDOT:PSS/ZnS/ P3HT hybrid solar cells for the future studies.

REFERENCES

Adaikalam, K., Ambika, N., Kim, M. R., Elanchezhiyan, J., Chae, Y., & Rhee, J. K. (2010). Chemical bath deposition and characterization of nanocrystalline ZnO thin films. *Materials Science-Poland, 28(2),* 513–522. Retrieved from http://www.materialsscience.pwr.wroc.pl/

Arenas, M. C., Mendoza, N., Cortina, H., Nicho, M. E., & Hu, H. (2010). Influence of poly3–octylthiophene (P3OT) film thickness and preparation method on photovoltaic performance of hybrid ITO/CdS/P3OT/Au solar cells. *Solar Energy Materials & Solar Cells, 94,* 29–33. doi:10.1016/j.solmat.2009.04.013

Aydin Yüksel, S., Güneş, S., & Güney, H. Y. (2013). Hybrid solar cells using CdS thin films deposited via spray pyrolysis technique. *Thin Solid Films, 540,* 242–246. doi:10.1016/j.tsf.2013.05.126

Bozkurt Çırak, B., Eden, Ç., Erdoğan, Y., Demir, Z., Özdokur, K. V., Çağlar, B., … Çırak, Ç. (2020). The enhanced light harvesting performance of dye–sensitized solar cells based on ZnO nanorod–TiO_2 nanotube hybrid photoanodes. *Optik - International Journal for Light and Electron Optics, 203,* 163963. doi:10.1016/j.ijleo.2019.163963

Chen, F., Qiu, W., Chen, X., Yang, L., Jiang, X., Wang, M., & Chen, H. (2011). Large–scale fabrication of CdS nanorod arrays on transparent conductive substrates from aqueous solutions. *Solar Energy, 85,* 2122–2129. doi:10.1016/j.solener.2011.05.020

Christoph, J. B. (2004). Organic photovoltaics: technology and market. *Solar Energy Materials and Solar Cells, 83(2–3),* 273–292. doi:10.1016/j.solmat.2004.02.030

Chuu D. -S., & Dai C. -M. (1992). Quantum size effects in CdS thin films. *Physical Review B: Condensed Matter and Materials Physics, 45(20),* 11805–11810. doi:10.1103/PhysRevB.45.11805

Deng, D., & Chen, F. (2013). Preparation and photovoltaic properties of the composite based on CdS nanorod arrays and PCPDTBSe. *Journal of Materials Science: Materials in Electronics, 24,* 2072–2076. doi:10.1007/s10854-012-1058-1

Dou, L., Liu, Y., Hong, Z., Li, G., & Yang, Y. (2015). Low–Bandgap near–IR conjugated polymers/molecules for organic electronics. *Chemical Reviews, 115,* 12633–12665. doi:10.1021/acs.chemrev.5b00165

Green, M. A., Emery, K., Hishikawa, Y., Warta, W., & Dunlop, E. D. (2014). Solar cell efficiency tables (version 45). *Progress in Photovoltaics: Research and Applications 23(1),* 1–9. doi:10.1002/pip.2573

Ishwara, T. (2017). Comparison of TiO_2 Nanoporous Films in Hybrid Organic–inorganic Solar Cells. *Energy Procedia, 110,* 109–114. doi:10.1016/j.egypro.2017.03.114

Jabeen, U., Adhikari, T., Pathak, D., Shah, S. M., & Nunzi, J. -M. (2018). Structural, optical and photovoltaic properties of P3HT and Mn–doped CdS quantum dots based bulk hetrojunction hybrid layers. *Optical Materials, 78,* 132–141. doi:10.1016/j.optmat.2018.02.019

Jabeen, U., Adhikari T., Shah, S. M., Pathak, D., Wagner, T., & Nunzi, J. -M. (2017). Photovoltaic performance of P3HT–porphyrin functionalized 1D CdS nanostructured organic inorganic bulk heterojunction hybrid solar cells. *The European Physical Journal Applied Physics, 78(3),* 34809. doi:10.1051/epjap/2017160491

Jia, Z., Wie, Y., Wang, X., Hu, S., Yao, K., & Li, F. (2016). Improvement of morphology and performance of P3HT/ZnO hybrid solar cells induced by liquid crystal molecules. *Chemical Physics Letters, 661,* 119–124. doi:10.1016/j.cplett.2016.08.062

Jiang, X., Chen, F., Qiu, W., Yan, Q., Nan, Y., Xu, H., … Chen, H. (2010). Effects of molecular interface modification in CdS/polymer hybrid bulk heterojunction solar cells. *Solar Energy Materials and Solar Cells, 94,* 2223–2229. doi:10.1016/j.solmat.2010.07.016

Khallaf, H., Oladeji, I. O., Chai, G., & Chow, L. (2008). Characterization of CdS thin films grown by chemical bath deposition using four different cadmium sources. *Thin Solid Films, 516(21),* 7306–7312. doi:10.1016/j.tsf.2008.01.004

Kim, Y. J., An, T. K., Oh, S. -J., Chung, D. S., & Park, C. E. (2014). Surface modification with MK–2 organic dye in a ZnO/P3HT hybrid solar cell: Impact on device performance. *APL Materials, 2(7),* 076108–076113. doi:10.1063/1.4886217

Kroon, R., Lenes, M., Hummelen, J. C., Blom, P. W. M., & de Boer, B. (2008). Small Bandgap Polymers for Organic Solar Cells (Polymer Material Development in the Last 5 Years). *Polymer Reviews, 48(3),* 531–582. doi:10.1080/15583720802231833

Lamouri, R., Salmani, E. M., Ez-zahraouy, H., & Benyoussef, A. (2016). Band–gap engineering of CdS, CdSe and ZnSe first–principles calculations. *2016 International Renewable and Sustainable Energy Conference (IRSEC), Marrakech, Morocco*. doi:10.1109/IRSEC.2016.7983969

Lim, E. L., Yap, C. C., Yahaya, M., & Salleh, M. M. (2013). Enhancement of ZnO nanorod arrays–based inverted type hybrid organic solar cell using spin–coated Eosin–Y. *Semiconductor Science and Technology, 28,* 045009–045014. Retrieved from https://iopscience.iop.org/

Lin, Y. -J. [Yow-Jon], You, C. -F., Chang, H. -C., Liu, C. -J., & Wu, C. A. (2015). Effects of sulfide treatment on the photoluminescent and structural properties of electrodeposited CdS films. *Journal of Luminescence, 158,* 407–411. doi:10.1016/j.jlumin.2014.10.051

Lin, Y. -Y. [Yun-Yue], Chu, T. -H., Li, S. -S., Chuang, C. -H., Chang, C. -H., Su, W. -F., … Chen, C. -W. (2009). Interfacial Nanostructuring on the Performance of Polymer/TiO_2 Nanorod Bulk Heterojunction Solar Cells. *Journal of the American Chemical Society, 131,* 3644–3649. doi:10.1021/ja8079143

Nan, Y. -X., Li, J. -J., Fu, W. -F., Qiu, W. -M., Zuo, L. -J., Pan, H. -B., … Chen, H. -Z. (2013). Performance enhancement of CdS nanorod arrays/P3HT hybrid solar cells via N719 dye interface modification. *Chinese Journal of Polymer Science, 31(6),* 879–884. doi:10.1007/s10118-013-1274-z

Pan, J. (2009). *Material Property Study on Dye Sensitized Solar Cells and Cu(Ga,In)Se_2 Solar Cells* (Master Thesis). Retrieved from https://etd.ohiolink.edu/

Pei, J., Hao, Y. Z., Lv, H. J., Sun, B., Li, Y. P., & Guo, Z. M. (2016). Optimizing the performance of TiO_2/P3HT hybrid solar cell by effective interfacial modification. *Chemical Physics Letters, 644,* 127–131. doi:10.1016/j.cplett.2015.11.058

Perednis, D., & Gauckler, L. J. (2005). Thin Film Deposition Using Spray Pyrolysis. *Journal of Electroceramics, 14(3),* 103–111. doi:10.1007/s10832-005-0870-x

Ruankham, P., Macaraig, L., Sagawa, T., Nakazumi, H., & Yoshikawa, S. (2011). Surface modification of ZnO nanorods with small organic molecular dyes for polymer–inorganic hybrid solar cells. *The Journal of Physical Chemistry C, 115 (48),* 23809–23816. doi:10.1021/jp204325y

Ruankham, P., Yoshikawa, S., & Sagawa, T. (2013). Effects of the morphology of nanostructured ZnO and interface modification on the device configuration and charge transport of ZnO/polymer hybrid solar cells. *Physical Chemistry Chemical Physics, 15(24),* 9516–9522. doi:10.1039/C3CP50266J

Thambidurai, M., Murugan, N., Muthukumarasamy, N., Agilan, S., Vasantha, S., & Balasundaraprabhu, R. (2010). Influence of the Cd/S Molar Ratio on the Optical and

Structural Properties of Nanocrystalline CdS Thin Films. *Journal of Materials Science & Technology, 26(3),* 193–199. doi:10.1016/S1005-0302(10)60032-1

Thitima, R., Patcharee, C., Takashi, S., & Susumu, Y. (2009). Efficient electron transfers in ZnO nanorod arrays with N719 dye for hybrid solar cell. *Solid-State Electronics, 53(2),* 176–180. doi:10.1016/j.sse.2008.10.014

Töreli, S. B. (2018). *Investigation of Some Physical Properties of Ga-Doped and (Ga-K)-Co-Doped CdS Thin Films* (Master Thesis). Retrieved from https://tez.yok.gov.tr/UlusalTezMerkezi

Urgessa, Z. N., Ruess, R., Tankio Djiokap, S. R., Botha, J. R., & Schlettwein, D. (2019). Effect of morphology and surface treatment on the performance of ZnO nanorod–based dye–sensitized solar cells. *Journal of Alloys and Compounds, 798,* 249–256. doi:10.1016/j.jallcom.2019.05.298

Wright, M., & Uddin, A. (2012). Organic—inorganic hybrid solar cells: A comparative review. *Solar Energy Materials & Solar Cells, 107,* 87–111. doi:10.1016/j.solmat.2012.07.006

Yang, C., Li, M., Zhang, W. -H., & Li, C. (2013). Controlled growth, properties, and application of CdS branched nanorod arrays on transparent conducting oxide substrate. *Solar Energy Materials & Solar Cells, 115,* 100–107. doi:10.1016/j.solmat.2013.03.023

Yılmaz, S. (2015). The investigation of spray pyrolysis grown CdS thin films doped with flourine atoms. *Applied Surface Science, 357(A),* 873–879. doi:10.1016/j.apsusc.2015.09.098

Yılmaz, S., Atasoy, Y., Tomakin, M., & Bacaksız, E. (2015). Comparative studies of CdS, CdS:Al, CdS:Na and CdS:(Al–Na) thin films prepared by spray pyrolysis. *Superlattices and Microstructures, 88,* 299–307. doi:10.1016/j.spmi.2015.09.021

Yılmaz, S., Töreli, S. B., Polat, İ., Olgar, M. A., Tomakin, M., & Bacaksız, E. (2017). Enhancement in the optical and electrical properties of CdS thin films through Ga and K co–doping. *Materials Science in Semiconductor Processing, 60,* 45–52. doi:10.1016/j.mssp.2016.12.016

Yılmaz, S., Ünverdi, A., Tomakin, M., Polat, İ., & Bacaksız, E. (2019). Surface modification of CBD-grown CdS thin films for hybrid solar cell applications. *Optik - International Journal for Light and Electron Optics, 185,* 256–263. doi:10.1016/j.ijleo.2019.03.156

Zhong, M., Yang, D., Zhang, J., Shi, J., Wang, X., & Li, C. (2012). Improving the performance of CdS/P3HT hybrid inverted solar cells by interfacial modification. *Solar Energy Materials and Solar Cells*, *96*, 160–165. doi:10.1016/j.solmat.2011.09.041

Zhong, P., Que, W. X., Zhang, J., Yuan, Y., Liao, Y. L., Yin, X. T., … Hu, X. (2014). Enhancing the performance of poly(3-hexylthiophene)/ZnO nanorod arrays based hybrid solar cells through incorporation of a third component. *Science China Physics, Mechanics & Astronomy*, *57*, 1289–1298. doi:10.1007/s11433-013-5213-3

Zhu, J. -J., Fan, G. -Q., Wei, H. -X., Li, Y. -Q., Lee, S. -T., & Tang, J. -X. (2012). Solution–processed inverted polymer solar cells using chemical bath deposited CdS films as electron collecting layer. *CrystEngComm*, *14*, 8090–8096. doi:10.1039/C2CE25698C

CURRICULUM VITAE

Personal Informations

SURNAME, Name	: ÜNVERDİ, Ahmet
Birth date, place	: 06.01.1995, Adana – Turkey
E-Mail	: unverdiahm@hotmail.com

Education

Degree	**School/University – Department – GPA**	**Year**
Master's Degree (Current Thesis')	Adana Alparslan Türkeş Science and Technology University – *Nanotechnology and Engineering Sciences* ***(%100 English)*** – **3,14/4**	2017 – 2020
Bachelor's Degree (**ErasmusGermany**)	Technische Universität Ilmenau – *Elektrotechnik und Informationstechnik* ***(%100 German)*** – **3,10/4**	2014 – 2015
Bachelor's Degree	Karabük University – *Electrical & Electronics Engineering* ***(%100 English)*** – **3,27/4**	2013 – 2017
High school	Seyhan Danişment Gazi Anatolian High School – *Science Oriented* – **72/100**	2009 – 2013

Languages

Tongue	**Learning Style**	**Level**
Turkish	Mother Tongue	
English	Educational + Personal + in Germany	Advanced
Arabic	Family + Personal	Intermediate
German	Personal + Educational + in Germany	Intermediate
Russian	Personal	Beginner

Professional Interest Areas

Renewable Energy Systems	Electronic Card Design	Defense Industry
Space & Military Vehicles	Electric – Electronics	Management
Nanotechnology	Production – R&D	Sales

Computer Knowledge

VHDL Programming	(+)	MATLAB	(+)	LTSpice	(+)
Microsoft Office	(+++)	SketchUP	(+)	Proteus	(++)
AutoCAD	(++)	Altium	(+)	C++	(+)

PUBLICATIONS

A. SCI Publications

i. Yılmaz, S., Polat, İ., Tomakin, M., Ünverdi, A., & Bacaksız, E. (2019). Enhanced efficiency of CdS/P3HT hybrid solar cells via interfacial modification. *Turkish Journal of Physics, 43, 116–125*. doi:10.3906/fiz-1810-21

ii. Yılmaz, S., Ünverdi, A., Tomakin, M., Polat, İ., & Bacaksız, E. (2019). Surface modification of CBD-grown CdS thin films for hybrid solar cell applications. *Optik - International Journal for Light and Electron Optics, 185, 256–263*. doi:10.1016/j.ijleo.2019.03.156

iii. Yılmaz, S., Tomakin, M., Ünverdi, A., & Aboghalon, A. (2019). A Study on Hydrothermal Grown CdS Nanospheres: Effects of Cd/S Molar Ratio. *Gazi University Journal of Science. 32(4), 1271–1281*. doi:10.35378/gujs.513525

iv. Yılmaz, S., Tomakin, M., Ünverdi, A., Aydın, A., Polat, İ., & Bacaksız, E. (2020). Structural, morphological, optical analyses of Ni-doped CdS thin films and their photovoltaic performance in hybrid solar cells. *Journal of Materials Science: Materials in Electronics.* doi:10.1007/s10854-020-03846-1